Article

Immunity

Aged circulating CD8⁺ T cells and their secreted factors drive cognitive decline

Graphical abstract

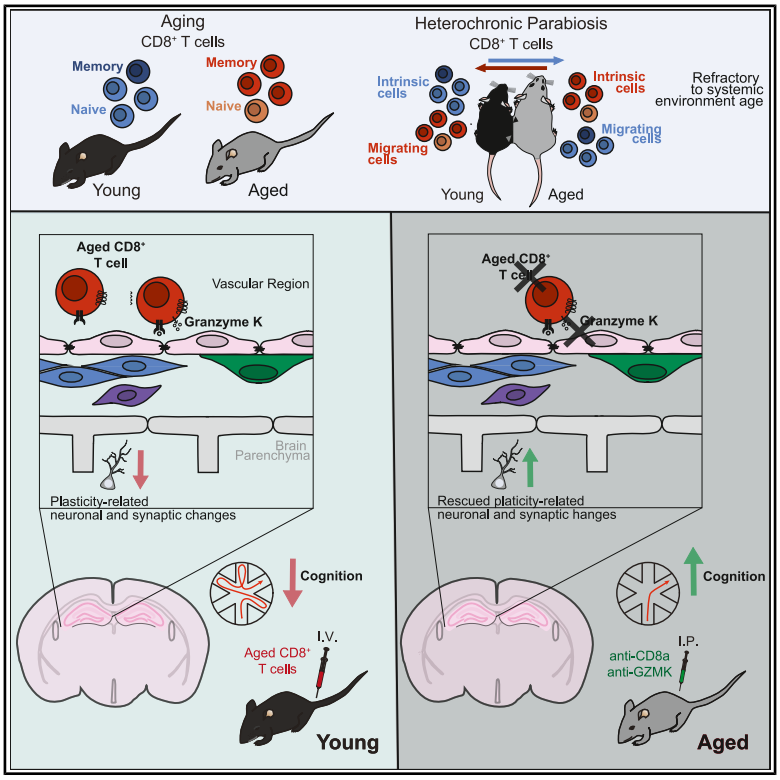

Highlights

- T cell population states are refractory to systemic environment age
- Aged circulating CD8⁺ T cells drive hippocampal-dependent cognitive decline
- Depleting or blocking activation of aged CD8⁺ T cells abrogates pro-aging effects
- Targeting aged CD8⁺ T cell-derived granzyme K rescues cognition

Authors

Juliana Sucharov, Gregor Bieri, Karishma J.B. Pratt, ..., Zachary J. Holmes, Julien Couthouis, Saul A. Villeda

Correspondence

saul.villeda@ucsf.edu

In brief

The role of non-infiltrating aged CD8⁺ T cells in brain function remains unclear. Sucharov et al. reveal that aged circulating cytotoxic T cells are drivers of age-related cognitive decline. Removal of aged T cells, or their secreted factor granzyme K, rescues cognition in mice. These findings have promise for therapeutics that target immune factors in circulation to restore brain function.

Sucharov et al., 2026, Immunity *59*, 1–16
June 9, 2026
https://doi.org/10.1016/j.immuni.2026.04.014

CellPress

Immunity

CellPress
OPEN ACCESS

Article

Aged circulating CD8+ T cells and their secreted factors drive cognitive decline

Juliana Sucharov,[1,2] Gregor Bieri,[1] Karishma J.B. Pratt,[1,3] Amber R. Philp,[1] Turan Aghayev,[1] Shanan Sahota,[1] Laura Remesal,[1] Adam B. Schroer,[1] Cedric E. Snethlage,[1,4] Rebecca Chu,[1,2] Zachary J. Holmes,[1,2] Julien Couthouis,[5] and Saul A. Villeda[1,2,3,4,6,7,8,*]

[1]Department of Anatomy, University of California, San Francisco, San Francisco, CA 94143, USA
[2]Biomedical Sciences Graduate Program, University of California, San Francisco, San Francisco, CA 94143, USA
[3]Developmental and Stem Cell Biology Graduate Program, University of California, San Francisco, San Francisco, CA 94143, USA
[4]Eli and Edythe Broad Center for Regeneration Medicine and Stem Cell Research, San Francisco, CA 94143, USA
[5]Department of Genetics, Stanford University School of Medicine, Stanford, CA 94305, USA
[6]Department of Physical Therapy and Rehabilitation Science, University of California, San Francisco, San Francisco, CA 94143, USA
[7]Bakar Aging Research Institute, University of California, San Francisco, San Francisco, CA 94143, USA
[8]Lead contact
*Correspondence: saul.villeda@ucsf.edu
https://doi.org/10.1016/j.immuni.2026.04.014

SUMMARY

Changes in peripheral CD8+ T cells are a hallmark of immune aging. However, the role of aged non-infiltrating CD8+ T cells in brain aging remains to be fully defined. Here, we showed that aged circulating CD8+ T cells and their secreted factors drove hippocampal-dependent cognitive decline. Using heterochronic parabiosis and transcriptomics analysis, we observed that peripheral CD8+ T cells maintained properties intrinsic to their age. Systemic exposure of young mice to aged CD8+ T cells elicited synaptic-related hippocampal changes and impaired cognition, and inhibiting activation, but not infiltration, mitigated their pro-aging effects. Conversely, targeting aged circulating CD8+ T cells restored youthful signatures and rescued cognition. Mechanistically, we identified granzyme K (GZMK) as a secreted pro-aging CD8+ T cell-derived factor in plasma, and GZMK inhibition rescued cognition in aged animals. Together, our data identified activated aged CD8+ T cell-derived circulating factors as potential therapeutic targets to rescue cognition in old age.

INTRODUCTION

Aging is associated with cognitive decline[1] and pro-aging systemic interventions promote cognitive dysfunction in young animals.[2,3] As such, it is essential to identify peripheral cellular and molecular drivers of age-related cognitive impairments as targets by which to restore cognition in old age. Interestingly, there are known age-related changes in the peripheral immune system[4–6] with an emerging role as a driver of brain dysfunction.[7–14] Indeed, the peripheral immune system is implicated in brain aging in the hippocampus, which is a master regulator of learning and memory.[15]

Transcriptional analyses of young and aged peripheral immune cells highlight changes in CD8+ T cells as a prominent hallmark of immune aging, with the emergence of an age-associated population characterized by expression of the serine protease granzyme K (GZMK).[16,17] In the brain, infiltrating CD8+ T cells in aged mice decrease adult neurogenesis in the subventricular zone of the lateral ventricles,[9] promote axon degeneration in the optic nerve,[12] and induce neuroinflammation in the white matter.[13] By contrast, only modest CD8+ T cell infiltration is reported in the aged hippocampus in the absence of neurodegenerative disease pathology in mouse models,[18,19] while analysis of postmortem human hippocampi finds no age-related changes in infiltration.[20] Notwithstanding, despite the vast majority of CD8+ T cells residing in the periphery, the role of aged non-infiltrating circulating CD8+ T cells or their secreted factors in hippocampal-dependent cognitive decline is yet to be fully defined. We therefore sought to investigate the effect of peripheral aged CD8+ T cells on the hippocampus and ascertain the rejuvenating potential of selectively targeting this immune cell population in circulation at old age.

Using heterochronic parabiosis, we demonstrated that aged circulating CD8+ T cells were refractory to a young systemic environment, maintaining properties intrinsic to their cellular age. Systemic exposure of young mice to aged circulating CD8+ T cells elicited hippocampal aging transcriptional signatures and cognitive decline, which were attenuated by blocking T cell activation. We further showed that targeting aged circulating CD8+ T cells restored synaptic-related hippocampal signatures and ameliorated age-related cognitive impairments. Mechanistically, we demonstrated that GZMK, secreted by age-associated CD8+ T cells, impaired cognitive function, and inhibition of systemic GZMK in aged mice restored cognition.

Please cite this article in press as: Sucharov et al., Aged circulating CD8+ T cells and their secreted factors drive cognitive decline, Immunity (2026), https://doi.org/10.1016/j.immuni.2026.04.014

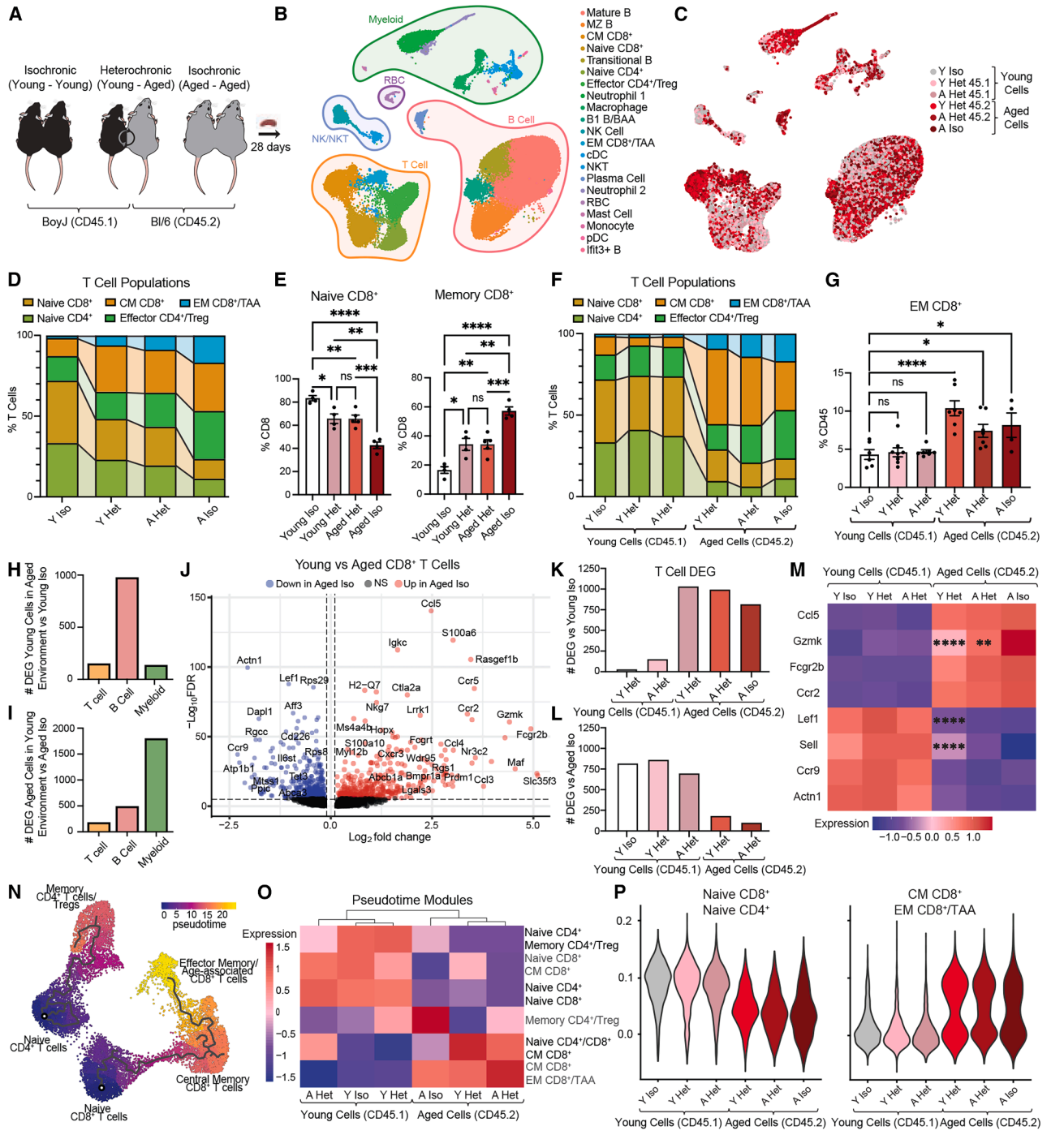

Figure 1. T cell populations are refractory to a rejuvenating or aging systemic milieu

(A) Schematic illustrating parabiosis pairs, followed by single-cell RNA sequencing (scRNA-seq) of splenocytes, sorted for CD45.1+ (4 months, BoyJ) or CD45.2+ (20 months Bl/6), (*n* = 4/group, combined after sorting).

(B and C) Uniform manifold approximation and projection (UMAP) of identified cell types (B) and of mouse identity of cell origin (C) (*n* = 1/group).

(D) Percentages of splenocyte T cell populations by scRNA-seq (*n* = 1/group).

(E) Flow cytometry confirmation of changes in naive (CD44−) and memory (CD44+) CD8+ T cell populations (*n* = 4/group).

(F) Percentages of splenocyte T cell populations by scRNA-seq, split by origin of cells (*n* = 1/group).

(G) Flow cytometry confirmation of changes in effector memory (CD62l−) CD8+ T cell populations (*n* = 4–7/group).

(H and I) Number of DEGs in different cell types in young cells (CD45.1) in the aged heterochronic animal vs. young isochronic control (H), or aged cells (CD45.2) in the young heterochronic animal vs. aged isochronic control (I) (*n* = 1/group).

(J) Volcano plot of DEGs in aged isochronic vs. young isochronic CD8+ T cells (*n* = 1/group).

(legend continued on next page)

Please cite this article in press as: Sucharov et al., Aged circulating CD8+ T cells and their secreted factors drive cognitive decline, Immunity (2026), https://doi.org/10.1016/j.immuni.2026.04.014

These findings identify activated aged circulating CD8+ T cells and their secreted factors as drivers of hippocampal-dependent cognitive decline in aging.

RESULTS

Peripheral T cell populations are largely refractory to a young or aged systemic milieu

Considering the pro-aging effects observed in the hippocampus following heterochronic parabiosis,[2,8,15,21] we first assessed changes in peripheral immune cell trafficking and transcriptional responses to young and aging systemic milieus using cellular indexing of transcriptomes and epitopes by sequencing (CITE-seq) analysis. Young (4 months) and aged (20 months) mice were surgically joined into isochronic (young-young and old-old) and heterochronic (young-old) parabiotic pairings for 28 days (Figure 1A). To distinguish young versus aged cells in heterochronic parabionts, young CD45.1 B6/BoyJ and aged CD45.2 B6 mice were joined (Figures 1A and S2B). We performed CITE-seq analysis on splenocytes of young isochronic, aged isochronic, young heterochronic, and aged heterochronic parabionts (Figures 1B and 1C). Signatures for each cluster were generated by differential gene expression analyses, and cell types were established based on transcriptomic signature and canonical surface markers (Figures S1A and S1B).

Consistent with age-related changes[17,22] (Figures S2A and S2D), we observed decreased naive CD4+ and CD8+ T cell populations, increased effector and memory CD4+ and CD8+ T cells, and the emergence of age-associated effector memory CD8+ T cells in aged isochronic compared with young isochronic parabionts (Figures 1D and 1E). In heterochronic parabiosis, we observed bidirectional trafficking of CD4+ and CD8+ T cells with the percentage of T cell populations reaching near equilibrium between young and aged parabionts (Figures 1D and 1E). Subsequently, we examined whether exposure to a young or aged systemic milieu altered the distribution of T cell populations intrinsic to their cellular age. We characterized T cells derived from young CD45.1 versus aged CD45.2 animals across isochronic and heterochronic parabiotic conditions and observed that age-related differences in the distribution of CD4+ and CD8+ T cell populations persisted irrespective of the age of the systemic milieu, which is contrary to other immune cell populations (Figures 1F, 1G, S1C–S1F, and S2C).

Next, we assessed whether exposure to a young or aged systemic milieu altered the transcriptome of CD8+ T cells. While exposure to a young or aged systemic milieu elicited prominent transcriptional changes in myeloid and B cells, the number of differentially expressed genes (DEGs) remained similar within young or aged CD8+ T cells, regardless of environment (Figures 1H, 1I, S1L, and S1M). Prominent age-dependent transcriptional changes were detected in CD8+ T cells from young compared with aged isochronic parabionts (Figure 1H); however, those changes persisted in young and aged cells across heterochronic conditions (Figures 1K, 1L, S1G, and S1H). Moreover, in aged CD45.2 CD8+ T cells, increased expression of age-associated effector memory T cell markers (e.g., *GZMK*) and decreased expression of naive T cell markers (e.g., *Lef1* and *Sell*) were observed regardless of the age of the systemic milieu, and few significant changes in expression occurred compared with the age-matched control (Figure 1M). Additionally, we examined the transcriptional aging progression of T cells following parabiosis by pseudotime analysis and observed that pseudotime trajectories from naive to aging-associated effector memory states persisted in aged CD45.2 CD8+ T cells in both isochronic and heterochronic parabionts (Figures 1N–1P, S1N, and S1O). Collectively, these data suggest that CD8+ T cells maintain properties intrinsic to their cellular age, which are largely refractory to the effects of a young or aged systemic milieu over the time frame of parabiosis.

Circulating aged CD8+ T cells alter hippocampal transcriptional profiles and impair cognition

Having determined the refractory nature of aged CD8+ T cells to their systemic environment, we investigated the pro-aging potential of aged circulating CD8+ T cells on the young hippocampus. For this, we performed an adoptive transfer of aged (22 months) or young (4 months) CD8+ T cells into young (4 months) animals (Figures 2A, S3A, and S3B). Transferred young and aged CD8+ T cells were observed in the spleen at equal frequencies (Figure S3C). As a baseline for age-related changes, we assessed CD8+ T cell infiltration in the young and aged hippocampus and surrounding regions, and we observed the increased localization of CD8+ T cells in the vascular and perivascular spaces of the aged hippocampus, and in the vascular, perivascular, and parenchymal regions surrounding the aged hippocampus (Figures S2E–S2J). Minimal infiltration into the young hippocampus was detected following adoptive transfer (Figure S3D).

To investigate the molecular changes elicited in the young hippocampus by aged circulating CD8+ T cells, we performed bulk RNA sequencing (RNA-seq) analysis and detected differential expression of 2,080 genes relative to control animals. Overlaying significantly expressed DEGs from our bulk RNA-seq data over a single nucleus RNA-seq (snRNA-seq) hippocampal dataset (Table S1) identified that differential genes were significantly enriched in neuron and brain-barrier cell populations (Figure 2B). Gene Ontology (GO) analysis of upregulated and downregulated genes identified synaptic plasticity-related biological processes

(K and L) Number of DEGs in CD8+ T cells vs. the young isochronic control (K) or aged isochronic control (L) (n = 1/group).
(M) Heatmap of average expression of representative DEGs up- or down regulated in aged isochronic vs. young isochronic CD8+ T cells (n = 1/group). Stars represent significant differences from age-matched control.
(N) Pseudotime analysis of T cell populations overlaid on a UMAP projection of T cells (n = 1/group).
(O) Heatmap of pseudotime modules showing average expression of each module split by origin of cells and hierarchical clustering of cell origin (n = 1/group).
(P) Violin plot of pseudotime modules representing naive or memory CD8+ T cells, split by origin of cells (n = 1/group). Data are shown as mean ± SEM; *$p < 0.05$, **$p < 0.01$, ***$p < 0.001$, ****$p < 0.0001$. Statistical analysis was performed using one-way ANOVA with Tukey's post hoc (E) and (G) and DESeq2 (H)–(M). Data (A)–(P) represent one independent experiment.
See also Figures S1 and S2.

Please cite this article in press as: Sucharov et al., Aged circulating CD8+ T cells and their secreted factors drive cognitive decline, Immunity (2026), https://doi.org/10.1016/j.immuni.2026.04.014

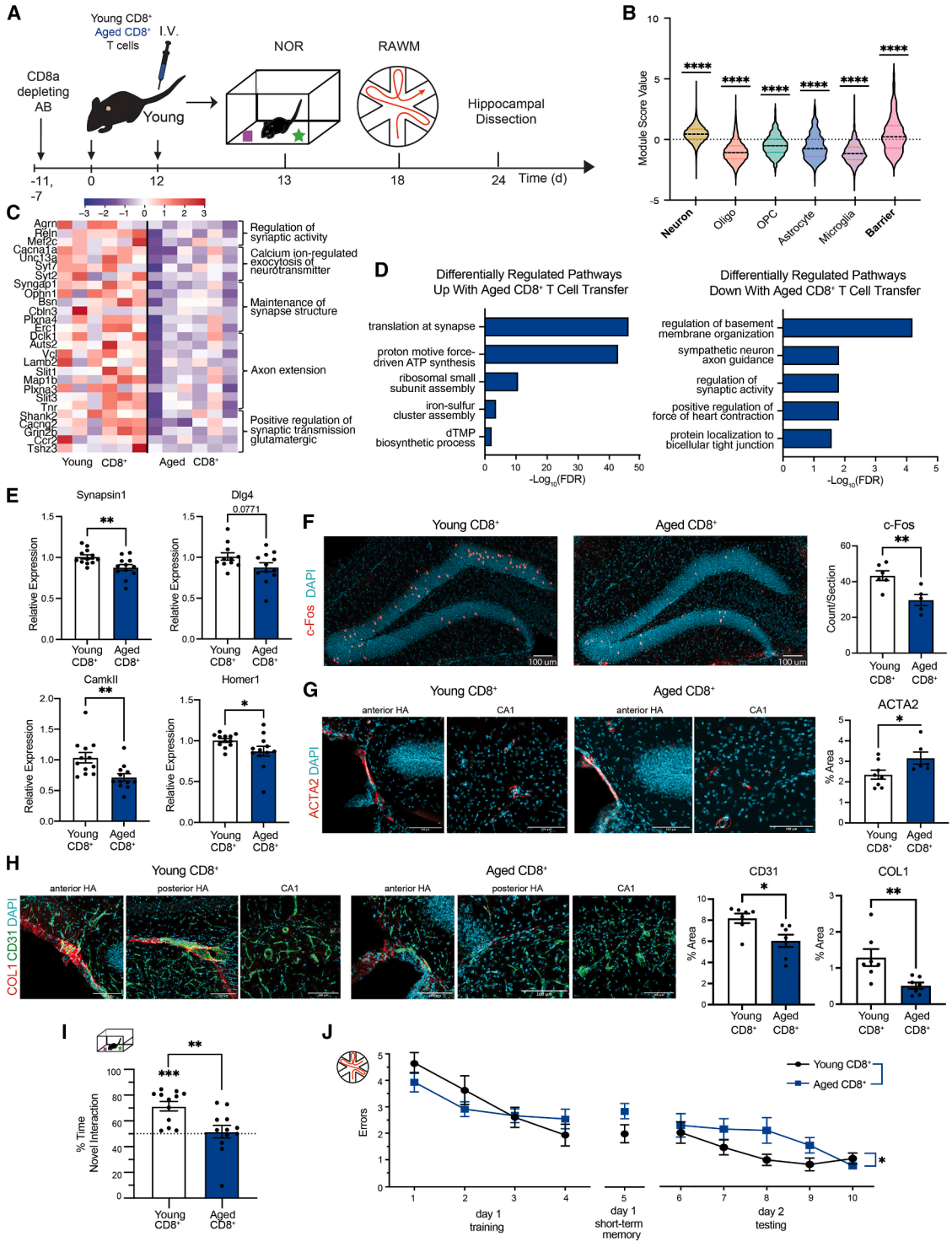

Figure 2. Aged circulating CD8+ T cells elicit aging transcriptional signatures in the young hippocampus and promote cognitive impairments

(A) Schematic illustrating the timeline of adoptive transfer of $3e^5$–$3e^6$ young (4 months) or aged (22 months) CD8+ T cells to young mice (4 months, BoyJ) after treatment with 200 ng CD8a-depletion antibody, intraperitoneally (i.p.), followed by cognitive testing (n = 12/group).

(B) Module score of DEGs ($p < 0.05$) in aged vs. young CD8+ transfer overlaid onto single nucleus RNA sequencing (snRNA-seq) to identify over-represented cell types (n = 6/group).

(C) Heatmap of representative DEGs in GO pathways related to synapses, along with the identified differentially regulated pathways (false discover rate [FDR] > 0.05) (n = 6/group).

(D) Top GO terms of biological processes associated with differentially expressed up- or downregulated genes (n = 6/group).

(legend continued on next page)

Please cite this article in press as: Sucharov et al., Aged circulating CD8+ T cells and their secreted factors drive cognitive decline, Immunity (2026), https://doi.org/10.1016/j.immuni.2026.04.014

(Figure 2C and 2D). Additionally, we detected decreased hippocampal expression of synaptic-plasticity-related genes *Synapsin1*, *Dlg4*, *CamkII*, and *Homer1* by quantitative PCR (qPCR), a decreased postsynaptic density protein 95 (PSD-95) protein and N-methyl-D-aspartate (NMDA) receptor subunit NR2B:NR2A ratio by western blot analysis, as well as a decreased number of neurons expressing the immediate early gene c-Fos in young mice exposed to aged circulating CD8+ T cells (Figures 2E, 2F, S4A, and S4B). In brain-barrier populations, young mice that received aged CD8+ T cells had decreased coverage of CD31 and collagen1 and increased coverage of actin alpha 2 (ACTA2) by immunohistochemistry (IHC) (Figures 2G, 2H, and S4C–S4H). Additionally, we detected decreased zonula occludens-1 (ZO-1) protein, a tight-junction protein, by western blot analysis (Figure S4A). No changes in microglial reactivity or inflammatory markers were observed by IHC or qPCR (Figures S4P–S4W).

At a functional level, hippocampal-dependent learning and memory were assessed using novel object recognition (NOR) and a radial arm water maze (RAWM). As a control for baseline age-related changes, cognitive performance was assessed in untreated young and aged mice, and characteristic age-related impairments were observed across behavioral tasks (Figures S5A–S5C). During NOR testing, young control mice exposed to young CD8+ T cells were biased toward a novel object relative to a familiar condition, whereas young mice exposed to aged CD8+ T cells showed no preference (Figure 2I). In the training phase of the RAWM paradigm, all mice showed a similar spatial learning ability regardless of adoptive transfer condition (Figure 2J). However, young mice exposed to aged CD8+ T cells demonstrated impaired learning and memory for the platform location during the testing phase of the task compared with young control mice exposed to young CD8+ T cells (Figure 2J). No difference in weight, activity as measured by distance traveled, or anxiety as measured by open field (OF) was observed between groups (Figure S5D). These behavioral data indicate that aged circulating CD8+ T cells are negative regulators of hippocampal-dependent learning and memory.

Inhibiting GPCR signaling of aged circulating CD8+ T cells abrogates pro-aging hippocampal effects

We next investigated how these aged CD8+ T cells functionally exerted their pro-aging effects on the young hippocampus. A variety of CD8+ T cell functions are dependent on $G\alpha_i$/o-coupled G protein-coupled receptor (GPCR)-mediated signaling, such as migration to lymph nodes where naive CD8+ T cells become activated upon encountering their cognate antigen, migration along chemokine gradients to sites of secondary activation, and strong physical interactions with and migration across tissue barriers. Correspondingly, we pre-treated aged CD8+ T cells with pertussis toxin (PTx), a known inhibitor of Gi/o protein signaling,[23,24] to block these functions prior to adoptive transfer. Specifically, we performed an adoptive transfer of PTx or vehicle-treated old (26 months) CD8+ T cells and vehicle-treated young CD8+ T cells into age-matched young (5 months) mice (Figure 3A).

PTx pre-treatment prevents T cell migration to lymph nodes without altering migration to open circulation tissues such as spleen, bone marrow, or liver.[23,24] Moreover, the time frame used for our studies was selected to be in line with previous reports showing minimal entry into the brain parenchyma with no impact on migration to the brain by PTx treatment.[15,24] Concordantly, we observed a decreased frequency of infiltrating CD8+ T cells into lymph nodes and an increased frequency in blood circulation, but detected no differences in migration to the spleen or brain between treatment groups (Figures 3B–3D). While age-related shifts from naive to effector memory CD8+ T cells were observed between vehicle-treated young and aged CD8+ T cells following adoptive transfer to young animals, these shifts were abrogated in the spleen of young animals following adoptive transfer of PTx-treated aged CD8+ T cells and *in vitro* upon co-culture with brain endothelial cells (Figures 3E, S3E, and S3F).

To investigate the impact on the young hippocampus, we performed snRNA-seq analysis. Nuclei were isolated from the hippocampi of all treatment groups (Figures 3A, 3F, and 3G). Signatures for each cluster were generated by DEG analyses, and cell types were established based on transcriptomic signatures and canonical markers[25] (Figures S6A and S6B). We detected prominent transcriptional changes in the hippocampus of young mice following adoptive transfer with vehicle-treated aged compared with young CD8+ T cells, which were in large part restored toward young control conditions in the PTx-treated group (Figures 3H, 3J, S6E, and S6F). We found that transcriptional responses in the young hippocampus following adoptive transfer were prominently observed across excitatory neuronal populations (dentate gyrus [DG], CA1, and CA2/CA3) (Figures 3I and 3J; Table S3). DEGs were largely unique to cell type (Figures 3K, 3L, S6C, and S6D). GO analysis of overlapping DEGs in excitatory neuronal populations driven by aged CD8+ T cells and rescued by PTx treatment identified synaptic- and metabolic-related biological processes (Figure 3M), in which

(E) Synapse-related gene expression as measured by quantitative reverse-transcription PCR (RT-qPCR) (n = 12/group).
(F) Representative image and quantification of c-Fos (red) expression in hippocampi of mice receiving young or aged CD8+ T cells as measured by immunohistochemistry (n = 5–6/group).
(G) Representative image in key areas of expression and quantification of ACTA2 (red) in the full hippocampi as measured by immunohistochemistry (n = 6–8/group).
(H) Representative image in key areas of expression and quantification of collagen1 (red) and CD31 (green) in the full hippocampi as measured by immunohistochemistry (n = 7/group).
(I) Object recognition memory as assessed by NOR and quantified as percent time spent exploring the novel object (n = 12/group).
(J) Hippocampal-dependent learning and memory as evaluated by RAWM. Changes in cognition were quantified as number of errors while attempting to find the goal arm (n = 12/group). Data are represented as mean ± SEM; scale bars represent 100 μm (F–H); *p < 0.05, **p < 0.01, ***p < 0.001, ****p < 0.0001. Statistical analysis was performed using one-sample t test vs. 0 (B) or vs. 50% (I), Fisher's exact tests (D), two-tailed t test (E–I), and two-way ANOVA with Tukey's post hoc (J). Data in (A)–(J) represent one independent experiment.
See also Figures S2–S5; Table S1.

Please cite this article in press as: Sucharov et al., Aged circulating CD8+ T cells and their secreted factors drive cognitive decline, Immunity (2026), https://doi.org/10.1016/j.immuni.2026.04.014

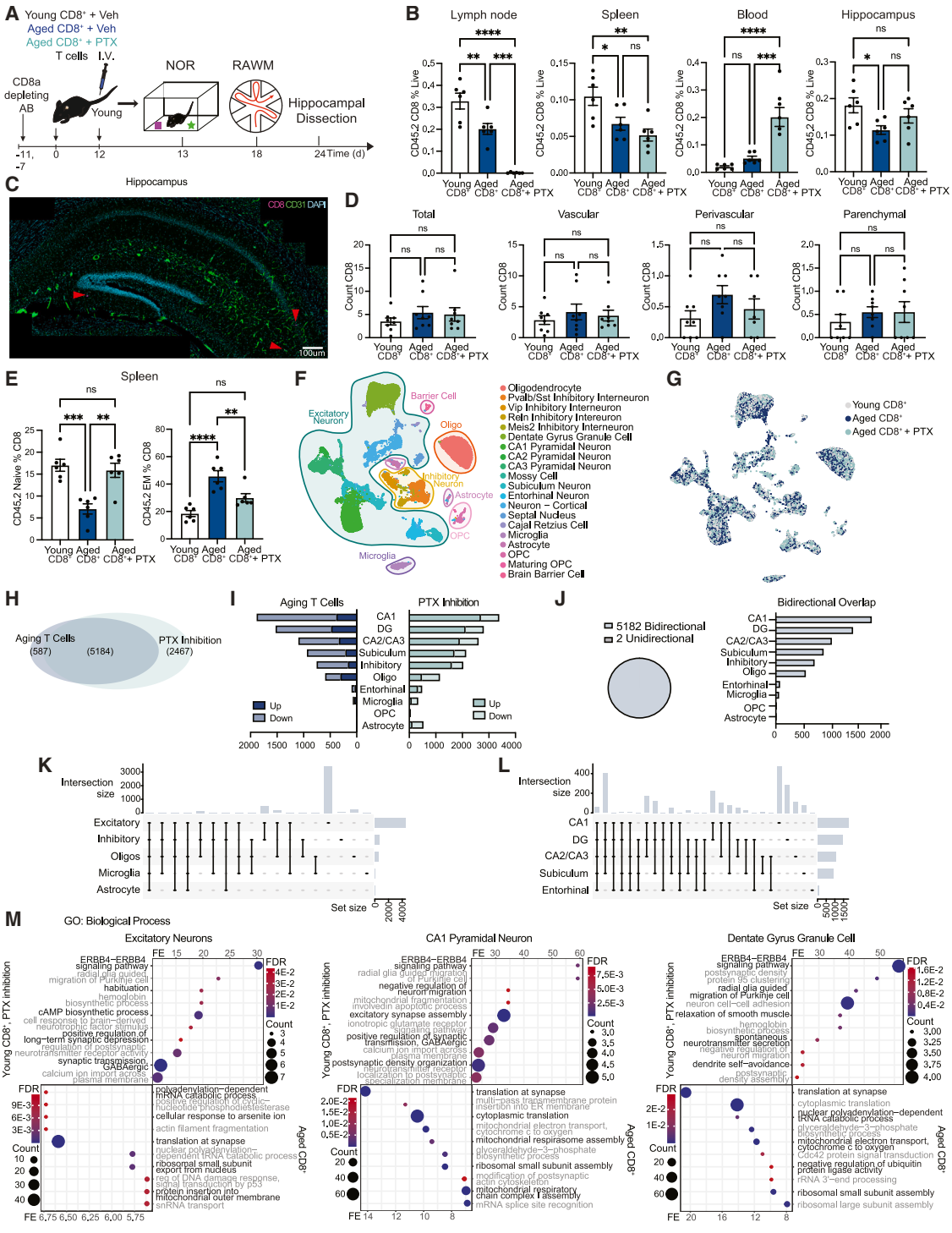

Figure 3. Pro-aging hippocampal effects of aged CD8+ T cells are dependent on GPCR signaling

(A) Schematic illustrating the timeline of adoptive transfer of $3e^5$–$3e^6$ young (5 months) vehicle-treated, aged (24–28 months) vehicle-treated, or aged PTx-treated CD8+ T cells to young mice (5 months, BoyJ) after treatment with 200 ng CD8a-depletion antibody, i.p., followed by cognitive testing (n = 11–12/group).

(B) Percentages of donor cells (CD45.2+CD3+CD8+) identified in lymph nodes, spleen, blood, and hippocampus 24 days after adoptive transfer (n = 6/group).

(C and D) Representative image (C) and quantification (D) of CD8+ cells (red) in the hippocampus localized in the total area or the vascular, perivascular, or parenchymal regions identified by localization with CD31 (green) as measured by immunohistochemistry (n = 8/group). Data represents n = 2 technical replicates.

(E) Percentage of splenocyte populations of naive (CD44−CD62l+) or effector memory (EM; CD44−CD62l−) donor CD8+ T cells identified by flow cytometry (n = 6/group).

(legend continued on next page)

Please cite this article in press as: Sucharov et al., Aged circulating CD8+ T cells and their secreted factors drive cognitive decline, Immunity (2026), https://doi.org/10.1016/j.immuni.2026.04.014

aged CD8+ T cell-driven transcriptional signatures elicited in excitatory neurons were restored to more youthful profiles by blocking T cell GPCR signaling (Figures S6F and S6I). Analysis of microglial populations identified changes in synaptic-related genes, rather than the typical aging-associated profile of inflammation and activation (Figures S6G and S6H).

Blocking activation, and not entry into tissue, mitigates the pro-aging cognitive effects of aged circulating CD8+ T cells

We next examined whether blocking CD8+ T cell GPCR signaling could mitigate the pro-aging cognitive effects of aged CD8+ T cells (Figure 4A). Hippocampal-dependent learning and memory were assessed using RAWM. Young control mice exposed to vehicle-treated young CD8+ T cells committed fewer errors locating the hidden platform compared with young mice exposed to vehicle-treated aged CD8+ T cells (Figure 4B). Congruent with snRNA-seq analysis, young mice exposed to PTx-treated aged CD8+ T cells exhibited no cognitive impairments in hippocampal-dependent spatial memory (Figure 4B). No differences in weight, activity metrics, or anxiety-related behaviors were observed between groups (Figure S5E). To further investigate the role of aged CD8+ T cell activation, we performed a complementary behavioral study in which young and aged CD8+ T cells were activated *in vitro* by CD3/CD28 co-stimulation prior to adoptive transfer to young mice (Figure S5F). An additional group was included in which activated aged CD8+ T cells were treated with PTx. During RAWM testing, young mice exposed to activated aged CD8+ T cells committed more errors compared with young mice exposed to activated young CD8+ T cells regardless of PTx treatment (Figure S5G). Treatment of young mice with young CD8+ T cells or young CD8+ T cells treated with PTx exhibited no behavioral changes compared to a saline treatment control (Figures S5H and S5I). Together, these data indicate that activation of aged CD8+ T cells is a driver of cognitive decline.

To delineate the role of activation in mediating the pro-aging cognitive effects of aged circulating CD8+ T cells, we treated aged CD8+ T cells *ex vivo* with tofacitinib, a Janus kinase (JAK)-signal transducer and activator of transcription (STAT) pathway (JAK-STAT) inhibitor, to block secondary CD8+ T cell activation and cytokine release, or with an anti-very late activation antigen-4 (VLA-4) antibody to block strong CD8+ T cell-barrier interaction and subsequent entry into tissue (Figures 4C and 4D). Treatment with either drug did not alter T cell phenotypes compared to the young control; however, treatment with tofacitinib resulted in shifts toward the young phenotype compared with the aged control (Figures S3G and S3H). Young mice exposed to vehicle-treated aged CD8+ T cells made significantly more errors before identifying the hidden platform (Figure 4E and 4F). Inhibiting activation and cytokine release by tofacitinib treatment, and not entry into tissue by anti-VLA-4 antibody treatment, mitigated aged CD8+ T cell-driven cognitive deficits (Figures 4E and 4F). No differences in activity metrics or anxiety-related behaviors were observed between groups (Figure S5J). Together, these behavioral data indicate that migration to the hippocampus, but not into the parenchymal tissue, and subsequent activation of T cells are necessary, at least in part, for the pro-aging effects of aged circulating CD8+ T cells on the hippocampus.

Targeting aged circulating CD8+ T cells restores hippocampal transcriptional profiles and improves cognition at old age

Having observed the pro-aging effects of aged circulating CD8+ T cells on hippocampal-dependent cognitive function, we explored the possibility that targeting CD8+ T cells could rescue cognition in aged mice. We employed a genetic model in which the absence of transporter associated with antigen processing 1 (TAP1) results in reduced expression of class 1 surface molecules and a loss of CD8+ T cells[26] (Figure S3I). We assessed hippocampal-dependent learning and memory in young (3 months) and aged (20 months) *Tap1*-knockout ($Tap1^{-/-}$) and wild-type (WT) littermate control mice using RAWM. In young animals, we observed no difference in spatial learning and memory between $Tap1^{-/-}$ and WT controls during RAWM training or testing (Figure 5A). However, aged $Tap1^{-/-}$ mice committed fewer errors locating a hidden platform during RAWM testing compared with WT controls (Figure 5B), which indicates enhanced cognition in an age-dependent manner. Next, we performed bulk RNA-seq analysis of the hippocampus of aged $Tap1^{-/-}$ mice compared with aged WT controls (Figure S6J). The overlap of DEGs in aging identified a majority of bidirectional changes, with GO analysis of the overlapped DEGs highlighting immune and synapse-related pathways (Figures S6K and S6L).

To selectively target aged peripheral CD8+ T cells late in life, aged (22 months) mice were given intraperitoneal injections of a CD8a-depleting antibody or IgG2b isotype control (Figure 5C). While we observed a decrease in peripheral CD8+ T cells, no difference in the number of CD8+ T cells in the hippocampus was observed (Figures 5D, S4L, and S4M). To investigate molecular changes elicited in the aged hippocampus, we performed bulk RNA-seq analysis and detected differential expression of 1,488 genes in aged mice receiving a CD8a-depleting antibody relative to the IgG2b control. Overlaying significantly expressed genes from our bulk RNA-seq data over a snRNA-seq hippocampal dataset (Table S1) identified

(F and G) UMAP projection of identified cell types (D) and of mouse identity of cell origin of snRNA-seq of hippocampi from young mice receiving young vehicle-treated, aged vehicle-treated, or aged PTx-treated CD8+ T cells (n = 3/group, combined after sorting).
(H) Overlap between total DEGs in mice receiving young vs. aged vehicle-treated CD8+ T cells and mice receiving vehicle-treated aged vs. PTx-treated aged CD8+ T cells (FDR < 0.05) (n = 1/group).
(I) Number of genes per cell type driven by aged CD8+ T cells or PTx treatment (n = 1/group).
(J) Directionality and number of overlapped DEGs in excitatory neurons driven by aged CD8+ T cells or PTx treatment (n = 1/group).
(K and L) UpSet plots displaying shared and unique DEGs per cell type (K) and excitatory neuron subtype (L) (n = 1/group).
(M) Top GO terms of biological processes associated with overlapping DEGs (n = 1/group). Data are represented as mean ± SEM; scale bars represent 100 μm (C); $^{*}p < 0.05$, $^{**}p < 0.01$, $^{***}p < 0.001$, $^{****}p < 0.0001$. Statistical analysis was performed using one-way ANOVA with Tukey's post hoc (B), (D), and (E), DESeq2 (H)–(L), and Fisher's exact tests (M). Data (A–M) represent one independent experiment.
See also Figures S3, S5, and S6; Table S3.

Please cite this article in press as: Sucharov et al., Aged circulating CD8+ T cells and their secreted factors drive cognitive decline, Immunity (2026), https://doi.org/10.1016/j.immuni.2026.04.014

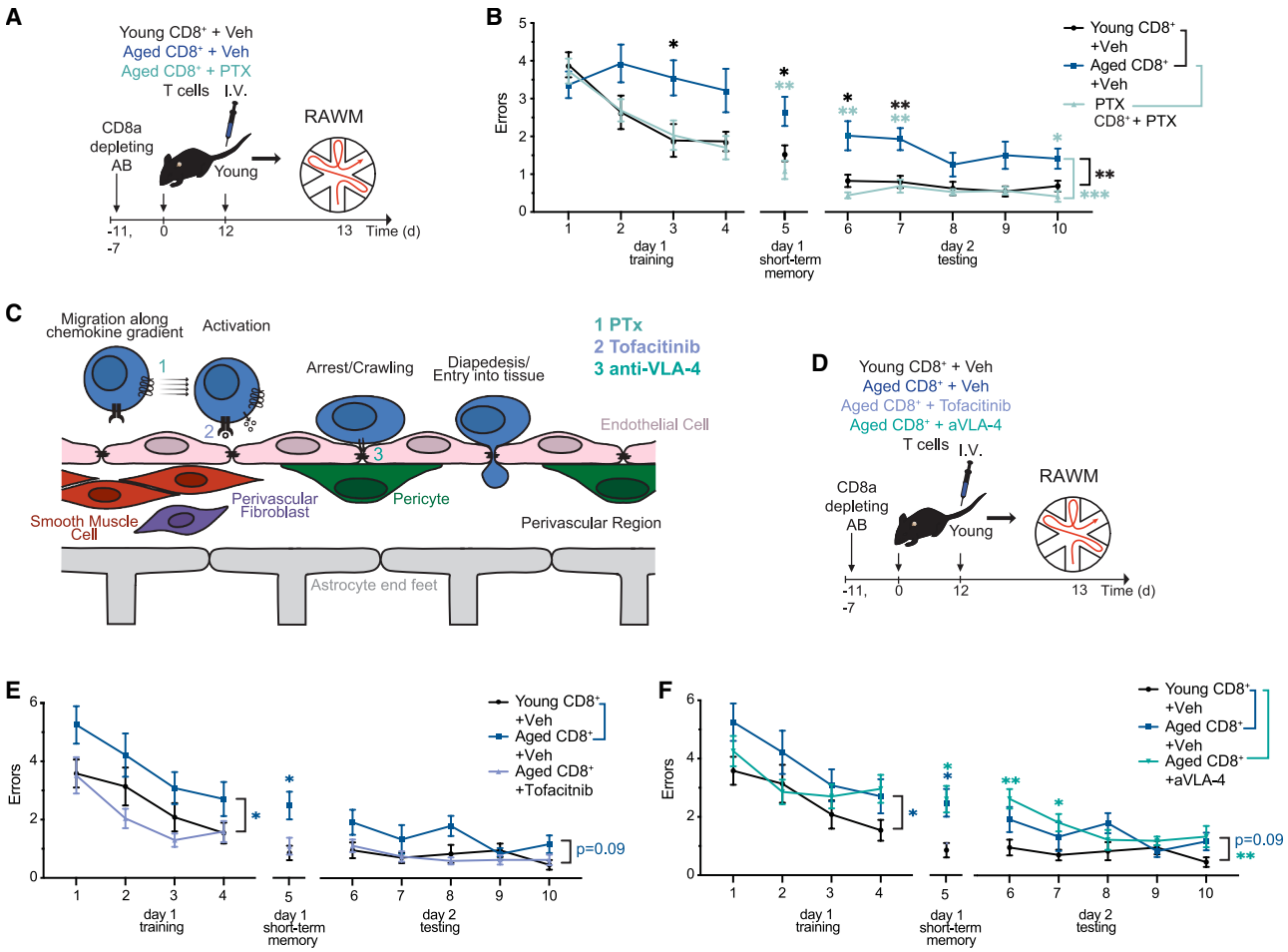

Figure 4. Activation of aged CD8+ T cells, rather than infiltration into tissue, is necessary for pro-aging cognitive effects

(A) Schematic illustrating the timeline of adoptive transfer of $3e^5$–$3e^6$ young (5 months) vehicle-treated, aged (24–28 months) vehicle-treated, or aged PTx-treated CD8+ T cells to young mice (5 months, BoyJ) after treatment with 200 ng CD8a-depletion antibody, i.p., followed by cognitive testing (n = 11–12/group).

(B) Hippocampal-dependent learning and memory as evaluated by RAWM (n = 11–12/group). Data (A and B) represent one independent experiment.

(C) Schematic representing CD8+ T cell functions inhibited by PTx (1), tofacitinib (2), or anti-VLA-4 (3).

(D) Schematic illustrating the timeline of adoptive transfer of $3e^5$–$3e^6$ young (4 months) vehicle-treated, aged (24 months) vehicle-treated, aged tofacitinib-treated CD8+ T cells, or aged anti-VLA-4-treated CD8+ T cells to young mice (4 months, BoyJ) after treatment with 200 ng CD8a-depletion antibody, i.p., followed by cognitive testing (n = 9/group).

(E and F) Hippocampal-dependent learning and memory as evaluated by RAWM after treatment with tofacitinib (E) or anti-VLA-4 (F) (n = 9/group). Data (D)–(F) represent one independent experiment. Data are represented as mean ± SEM; $*p < 0.05$, $**p < 0.01$, $***p < 0.001$. Statistical analysis was performed using two-way ANOVA with Šídák's post hoc (B), **(**E**)**, and **(**F**)**.

See also Figures S3 and S5.

that DEGs were enriched in neuronal populations (Figure 5E). GO analysis of up- and downregulated genes identified synaptic- and vascular-related biological processes (Figure 5F). Concordantly, we detected the increased expression of synaptic-plasticity-related genes *Synapsin1*, *Dlg4*, and *CamkII* by qPCR (Figure 5G), and increased synapsin 1 (SYN1) and PSD-95 proteins and NR2B:NR2A ratio by western blot analysis (Figures S4J and S4K). Additionally, analysis of vascular markers by IHC showed increased coverage of CD31 and decreased coverage of ACTA2, which suggested that the removal of systemic CD8+ T cells in aged animals may rescue some of the vascular changes driven by aged CD8+ T cells (Figure S4N and S4O). As with young mice exposed to aged CD8+ T cells, depletion of peripheral CD8+ T cells did not elicit changes in microglial reactivity (Figures S4X and S4Y).

To gain further cell-type-specific resolution, we performed snRNA-seq analysis of hippocampi from aged mice treated with CD8a-depleting antibody or isotype control (Figures 5H and 5I). We detected prominent transcriptional changes in excitatory neuronal populations and oligodendrocytes in the hippocampus of aged mice treated with CD8a-depleting antibody compared with isotype control (Figure 5J). Of the excitatory neuronal populations, we observed predominant transcriptional changes in DG and CA1 neurons (Figure 5K). We found that transcriptional responses following CD8+ T cell depletion were encoded in different cell types with genes that were largely unique

Please cite this article in press as: Sucharov et al., Aged circulating CD8+ T cells and their secreted factors drive cognitive decline, Immunity (2026), https://doi.org/10.1016/j.immuni.2026.04.014

CellPress
OPEN ACCESS

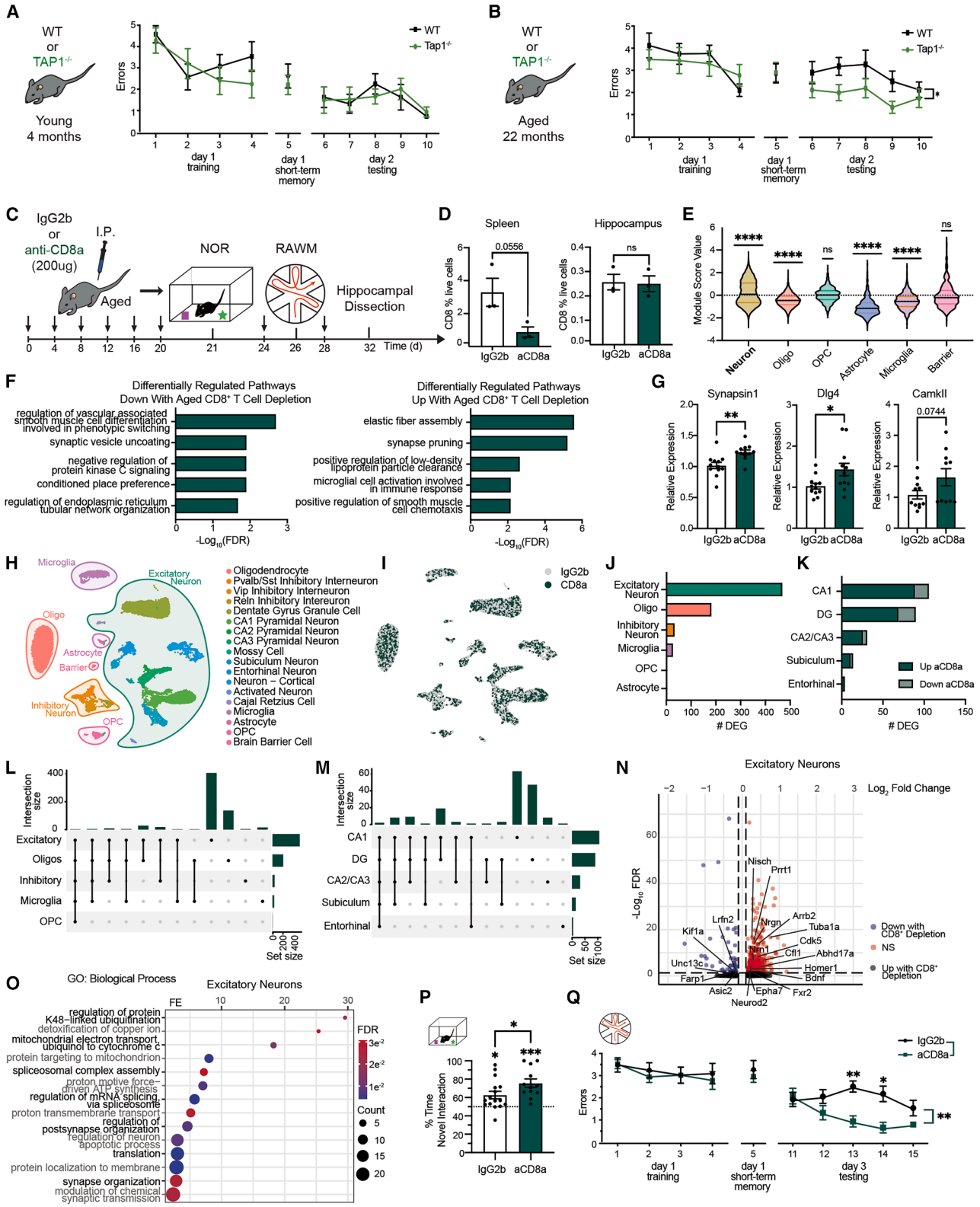

Figure 5. Depletion of circulating aged CD8+ T cells restores hippocampal transcriptional profiles and rescues cognition

(A) Representative schematic and hippocampal-dependent learning and memory of young (4 months) WT and TAP1$^{-/-}$ mice as evaluated by RAWM (n = 11/group).

(legend continued on next page)

Please cite this article in press as: Sucharov et al., Aged circulating CD8+ T cells and their secreted factors drive cognitive decline, Immunity (2026), https://doi.org/10.1016/j.immuni.2026.04.014

to their cell type (Figures 5L and 5M). GO analysis of DEGs in excitatory neuronal populations identified synaptic- and metabolic-related biological processes (Figures 5N and 5O).

To complement transcriptomics analysis, we assessed hippocampal-dependent learning and memory using NOR and RAWM. While both treatment groups showed a preference for the novel object during NOR testing, aged mice with depleted CD8+ T cells spent more time with the novel object compared with isotype control-treated mice (Figure 5P). Aged mice with depleted CD8+ T cells demonstrated improved memory for the platform location during the testing phase of the task compared with aged control mice (Figure 5Q). Aged mice with depleted CD8+ T cells also exhibited increased short-term memory during Y-maze testing but no change in amygdala-dependent associative memory during fear conditioning, which suggests a regional sensitivity to CD8+ T cell depletion (Figure S5L–S5N). No differences in well-being metrics, such as weight, activity, or anxiety-related behaviors were observed between groups (Figure S5K). Together, these data indicate that targeting aged peripheral CD8+ T cells restores synaptic-related transcriptional profiles and cognitive function in the aged hippocampus.

Targeting circulating GZMK ameliorates aging-associated hippocampal-dependent cognitive decline

Given the pro-aging effects of aged circulating CD8+ T cells, the possibility arises that systemic factors in circulation, which have been secreted by aged CD8+ T cells upon activation, could promote cognitive decline. Age-associated effector memory CD8+ T cells are the primary source of secreted GZMK in the aging systemic milieu,[16] and extracellular GZMK is implicated in promoting inflammation and senescence in the periphery.[27,28] Therefore, we elected to investigate the functional consequence of mimicking an age-related increase in systemic GZMK.

To begin, we confirmed that the age-related emergence of age-associated effector memory CD8+ T cell populations persisted in aged cells irrespective of the age of the systemic milieu (Figures 6A, 6B, and S1I). We corroborated increased GZMK expression exclusively in age-associated effector memory CD8+ T cells from isochronic parabionts (Figure 6C). We confirmed these changes by flow cytometry of cultured young and aged CD8+ T cells and observed an increased frequency of activated CD69+ CD8+ T cells and activated cells expressing GZMK (Figures 6D and S3K). To investigate the effect of CD8+ T cells expressing GZMK, we overexpressed GZMK or GFP control in young CD8+ T cells prior to adoptive transfer using a retroviral-mediated approach followed by cognitive testing by RAWM (Figures 6E and 6F). Young animals exposed to young CD8+ T cells expressing GZMK exhibited cognitive deficits in hippocampal-dependent spatial memory compared with GFP controls (Figure 6G).

Additionally, we observed increased circulating GZMK in plasma derived from aged compared with young mice by ELISA, as well as in plasma derived from young mice following adoptive transfer of aged CD8+ T cells, while this increase was no longer observed following adoptive transfer of PTx-treated aged CD8+ T cells (Figure 6H). To investigate the potential pro-aging activity of circulating GZMK on cognitive function, we used a hydrodynamic tail-vein injection (HDTVI)-mediated *in vivo* overexpression approach to increase circulating GZMK protein. To confirm increased expression in circulation, we generated expression constructs encoding a HiBiT-tagged version of GZMK. HiBiT is a small peptide that forms a complex with LgBiT to produce a luminescent signal,[29] which allows for the sensitive detection of tagged proteins.[14,29,30] Young (4 months) mice were given HDTVI with expression constructs encoding GZMK-HiBiT or GFP. An increased luminescent signal was confirmed in blood plasma and liver of GZMK-treated young animals (Figures 6I and S5O). Hippocampal-dependent learning and memory was assessed by RAWM in a larger cohort of young mice administered expression constructs encoding GZMK or GFP by HDTVI (Figure 6K). Increased systemic GZMK resulted in more errors committed locating a hidden platform during RAWM testing compared with young control mice (Figure 6L). Increased GZMK did not affect the metrics of well-being, such as weight and activity (Figure S5P). We also tested whether increasing systemic C-C motif chemokine ligand 5 (CCL5), the most significantly upregulated CD8+ T cell-derived secreted factor in our CITE-seq dataset (Figures 1H, S1J, and S1K), elicited pro-aging cognitive effects. Young mice were given HDTVI with expression constructs encoding either CCL5 or GFP control; however, no cognitive impairments were observed (Figure S5Q–S5T).

(B) Representative schematic and hippocampal-dependent learning and memory of aged (22 months) WT and TAP1$^{-/-}$ mice as evaluated by RAWM (n = 11/group). Data (A) and (B) represent one independent experiment.
(C) Schematic illustrating timeline of treatment of aged mice (22 months) with 200 ng CD8a-depletion antibody or IgG2b isotype control, i.p., followed by cognitive testing (n = 12–16/group).
(D) Numbers of CD8+ T cells in the spleen and hippocampus, as a percent of all live cells, measured by flow cytometry (n = 3/group).
(E) Module score of DEGs ($p < 0.05$) in CD8a-depletion hippocampi vs. isotype control, overlaid onto snRNA-seq to identify over-represented cell types (n = 5/group).
(F) Top GO terms of biological processes associated with differentially expressed up- or downregulated genes (FDR < 0.05) (n = 5/group).
(G) Synapse-related or inflammatory gene expression as measured by RT-qPCR (n = 12/group).
(H and I) UMAP of identified cell types (H) and of mouse identity of cell origin (I) of single nucleus RNA-seq of hippocampi from aged mice receiving CD8a-depleting antibody or isotype control (n = 3/group, combined after sorting).
(J and K) Number of DEGs per cell type (J), and number of up- or downregulated genes per excitatory neuron subtype (FDR < 0.05) (K) (n = 1/group).
(L and M) UpSet plots displaying shared and unique DEGs per cell type (L) and excitatory neuron subtype (M) (n = 1/group).
(N) Volcano plot of DEGs in excitatory neurons, with genes identified in synapse-related GO terms labeled (n = 1/group).
(O) Top GO terms of biological processes associated with DEGs in excitatory neurons (n = 1/group).
(P) Object recognition memory as assessed by NOR (n = 12–16/group).
(Q) Hippocampal-dependent learning and memory as evaluated by RAWM (n = 11–12/group). Data (C)–(Q) represent two independent experiments. Data are represented as mean ± SEM; $^{*}p < 0.05$, $^{**}p < 0.01$, $^{***}p < 0.001$, $^{****}p < 0.0001$. Statistical analysis was performed using two-way ANOVA with Šídák's post hoc (A), (B), and (Q), t test (D), (G), and (P), one-sample t test vs. 0 (E) or 50% (P), Fisher's exact tests (F) and (O), and DESeq2 (J)–(N).
See also Figures S3–S6; Table S1.

Please cite this article in press as: Sucharov et al., Aged circulating CD8+ T cells and their secreted factors drive cognitive decline, Immunity (2026), https://doi.org/10.1016/j.immunity.2026.04.014

CellPress
OPEN ACCESS

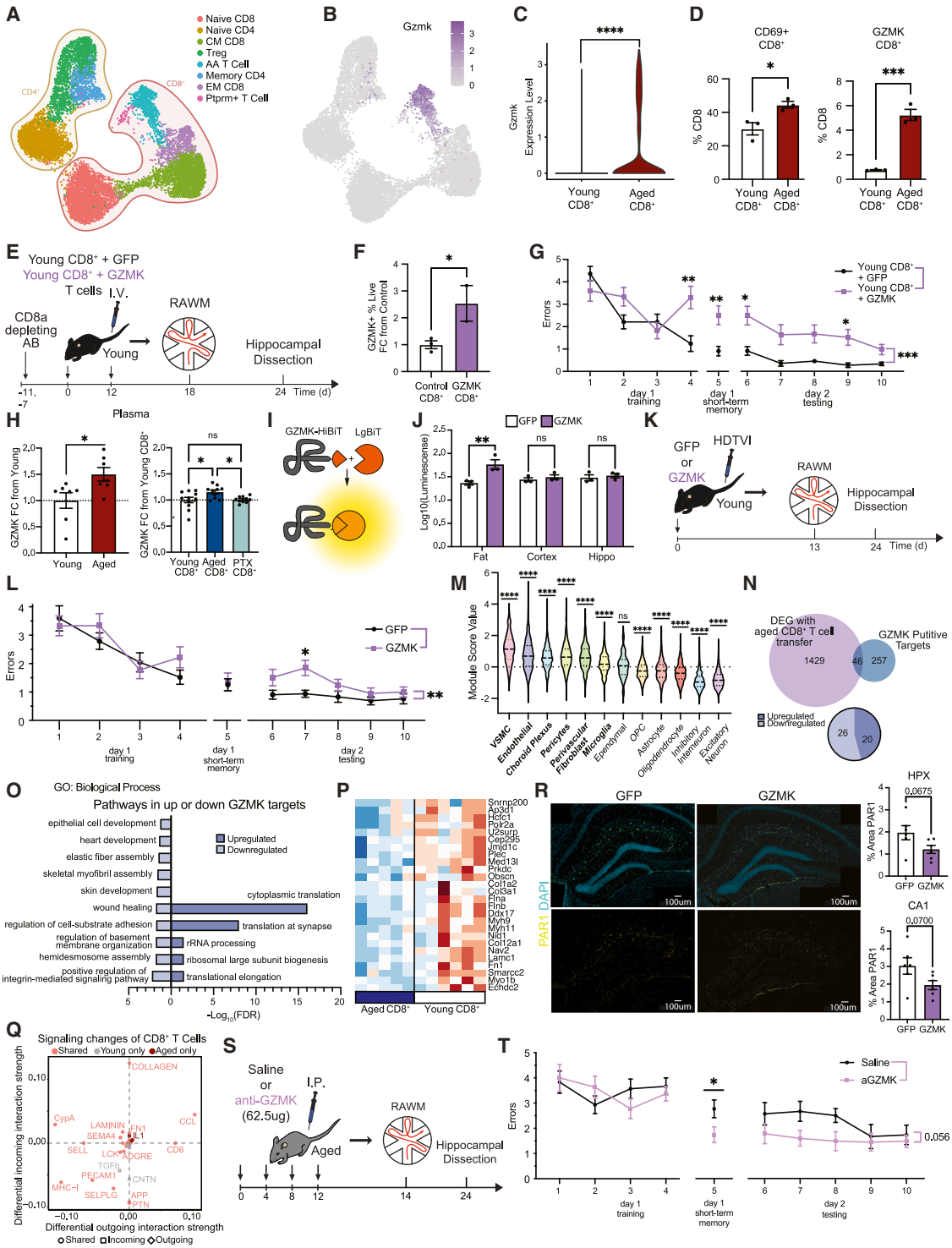

Figure 6. Aged CD8+ T cell-derived systemic GZMK promotes cognitive decline

(A) UMAP of identified T cell types (n = 1/group).

(B) Expression of GZMK in T cell types (n = 1/group).

(C) Violin plot of GZMK expression in young and aged isochronic CD8+ T cells (n = 1/group). Data (A)–(C) represent one independent experiment.

(D) Percentage of activated (CD69+) young and aged CD8+ T cells and activated cells expressing GZMK following 3 days in culture, as measured by flow cytometry (n = 3/group). Data represent one independent experiment.

(E) Schematic illustrating the timeline of adoptive transfer of $3e^5$ young (4 months) GFP or GZMK retrovirus-treated CD8+ T cells to young mice (4 months, BoyJ) after treatment with 200 ng CD8a-depletion antibody, i.p., followed by cognitive testing (n = 11/group).

(legend continued on next page)

Please cite this article in press as: Sucharov et al., Aged circulating CD8+ T cells and their secreted factors drive cognitive decline, Immunity (2026), https://doi.org/10.1016/j.immuni.2026.04.014

Together, these data indicate that selectively increasing circulating age-associated CD8+ T cell-secreted factor GZMK impairs cognitive function in the young hippocampus.

To ascertain the mechanisms of action, we measured the luminescence signal of GZMK-HiBiT in fat, cortex, and hippocampus. While tagged GZMK was identified in peripheral tissues, there was no detection in the hippocampus or cortex, which suggests that circulating GZMK did not readily cross the blood-brain barrier (Figure 6J). To identify potential cellular targets of circulating GZMK upstream of cognitive impairments, we overlaid previously reported putative GZMK substrates[27] over a snRNA-seq hippocampal and vascular dataset (Table S2). GZMK substrates were over-represented in many populations of barrier cells (e.g., vascular smooth muscle cells, endothelial cells, choroid plexus epithelial cells, pericytes, and perivascular fibroblasts) and under-represented in glial and neuronal populations (Figure 6M). Comparison of targets expressed within the hippocampus and DEGs in the hippocampus after systemic exposure to aged CD8+ T cells identified 46 overlapping substrates, and GO analysis of these overlapped genes identified a downregulation of various brain-border pathways (Figure 6N–6P). To further investigate, we utilized the Cell Chat package to assess potential signaling pathway changes between hippocampal cells and young or aged CD8+ T cells. While we identified changes in the reported pathways, such as increases in CCL and interleukin-1 (IL1) and decreases in selectin L (SELL) signaling, we also observed predicted changes in T cell-to-brain-barrier signaling pathways, such as collagen, fibronectin 1 (FN1), and laminin (Figure 6Q). Concordantly, we observed decreased coverage of proteinase-activated receptor 1 (PAR1), a GZMK target whose cleavage induces barrier cell dysfunction and alterations in epithelialization,[31,32] in young mice with increased systemic GZMK by IHC (Figure 6R). Taken together, these behavioral and transcriptomics data posit that cognitive impairments driven by aged CD8+ T cell-derived circulating GZMK are likely mediated, in part, through interactions with brain-barrier cells.

Last, we investigated the rejuvenating potential of targeting circulating GZMK at old age. For this, we utilized a GZMK inhibitor previously shown to rescue lung function in the context of airway inflammatory disease mouse models *in vivo*.[27] Aged (22 months) mice were given intraperitoneal injections of the GZMK inhibitor or vehicle control (Figure 6S), and hippocampal-dependent learning and memory was assessed by RAWM. Following GZMK inhibitor treatment, aged mice committed fewer errors locating a hidden platform during RAWM testing compared with vehicle-treated aged control mice (Figure 6T). These behavioral data indicate that systemically targeting extracellular GZMK in an aged animals can restore cognition.

DISCUSSION

Cumulatively, our data showed that activated aged circulating CD8+ T cells and their secreted factors were drivers of hippocampal-dependent cognitive decline. From a translational perspective, these data further suggested significant therapeutic potential to ameliorate age-related cognitive decline by targeting aged peripheral CD8+ T cell-derived factors in the blood circulation at old age.

While a prominent role is emerging for CD8+ T cells as regulators of brain aging,[33,34] thus far a focus has been placed predominantly on the role of CD8+ T cell infiltration and clonal expansion within the brain.[9,12,13,34–36] Perplexingly, infiltrating CD8+ T cells in the brain are ascribed contrasting detrimental and protective roles in mouse models of Alzheimer's disease pathology,[37–41] which underscores the need to delineate the role of infiltrating versus non-infiltrating CD8+ T cells in brain aging. Outside of the brain parenchyma, activation and immune surveillance of CD8+ T cells via the meningeal lymphatic network is disrupted in aging.[42] Moreover, single-cell RNA-seq analysis shows associations between altered cytokine signaling in effector memory CD8+ T cells in the cerebrospinal fluid of elderly humans and age-related cognitive impairments,[43] although no functional

(F) Percent of cells expressing GZMK day 5 post retroviral treatment vs. control, as measured by flow cytometry (n = 2–3/group).
(G) Hippocampal-dependent learning and memory as evaluated by RAWM (n = 11/group).
(H) ELISA of GZMK, as normalized to control in aged (22 months) vs. young (4 months) plasma and plasma of mice receiving young vehicle-treated vs. mice receiving vehicle- or PTx-treated aged CD8+ T cells (n = 7–10/group). Data (E)–(H) represent one independent experiment.
(I) Schematic illustrating HiBit reaction.
(J) Log10 transformed luminescence of HiBit-tagged GZMK in fat, cortex, and hippocampus 24 h post HDTVI (n = 3/group).
(K) Schematic illustrating the timeline of young mice (4 months) following systemic overexpression of GZMK or GFP via HDTVI followed by cognitive testing (n = 14–15/group).
(L) Hippocampal-dependent learning and memory as evaluated by RAWM (n = 14–15/group). Data (I–L) represent one independent experiment.
(M) Module score of putative GZMK targets, overlain onto single nucleus vessel RNA-seq (n = 2).
(N) Overlap of DEGs ($p < 0.05$) in aged vs. young CD8+ transfer hippocampi identified by bulk sequencing with putative GZMK targets expressed in the hippocampi (average expression > 1), and directionality of overlapped targets (n = 5–6/group).
(O) Top GO terms of biological processes associated with differentially expressed up- or downregulated overlapped targets (n = 5–6/group).
(P) Heatmap of differentially expressed downregulated GZMK targets (n = 5–6/group).
(Q) Predicted differential signaling pathways between young or aged CD8+ T cells and hippocampal cells by Cell Chat analysis (n = 3/group, combined). Data (M)–(Q) represent one independent experiment.
(R) Representative image and quantification of Par1 (yellow) in the full hippocampi and the CA1 region as measured by immunohistochemistry (n = 6/group). Data represent one independent experiment.
(S) Schematic illustrating the timeline of treatment of aged mice (22 months) with 62.5 μg anti-GZMK antibody or saline control, i.p., followed by cognitive testing (n = 9–10/group).
(T) Hippocampal-dependent learning and memory as evaluated by RAWM (n = 9–10/group). Data (S) and (T) represent one independent experiment. Data are represented as mean ± SEM; scale bars represent 100 μm (R); $^{*}p < 0.05$, $^{**}p < 0.01$, $^{***}p < 0.001$, $^{****}p < 0.0001$. Statistical analysis was performed using DESeq2 (C), (N), and (P), t test (D) and (R), one-way ANOVA with Tukey's post hoc (H), one-tailed t test (F), two-way ANOVA with Šídák's post hoc (G), (J), (L), and (T), one-sample t test vs. 50% (M), and Fisher's exact tests (O).
See also Figures S3 and S5; Table S2.

Please cite this article in press as: Sucharov et al., Aged circulating CD8+ T cells and their secreted factors drive cognitive decline, Immunity (2026), https://doi.org/10.1016/j.immuni.2026.04.014

studies accompany transcriptomic analyses. While we do not exclude a role for infiltrating CD8+ T cells in the aged hippocampus, our data defined an important mutually inclusive functional role for non-infiltrating aged circulating CD8+ T cells and their secreted factors in driving cognitive decline in the aging hippocampus.

We further identified age-associated effector memory CD8+ T cell-derived circulating factors, such as secreted GZMK, as systemic mediators of hippocampal aging. It has been suggested that GZMK, alone or in combination with interferon-γ, can enhance age-related inflammatory processes.[16,44] As such, age-associated CD8+ T cell-derived factors in blood may work in concert with infiltrating CD8+ T cells to promote localized interferon-γ-mediated pro-aging effects across diverse brain regions. Of note, infiltrating GZMK+ CD8+ T cells are detrimental in an Aβ-based Alzheimer's model by promoting neurotoxic inflammation, yet they are protective in a Tau-based Alzheimer's model by targeting microglia.[40,41] In this context, targeting CD8+ T cell-derived GZMK in circulation, rather than infiltrating GZMK+ CD8+ T cells themselves, provides a promising alternative therapeutic approach that is agnostic to brain region and disease state.

Mechanistically, we linked aged circulating CD8+ T cells to changes in the brain vasculature, which is in line with the emerging role of extracellular, secreted GZMK in affecting border-associated cells.[31,32,45–48] We demonstrate that selective manipulations of the brain vasculature drive both age-related decline and rejuvenation of hippocampal-dependent cognitive function.[49] Moreover, previous studies indicate that vascular manipulations regulate neuronal and regenerative functions in the brain.[3,50,51] In this context, our findings position aged circulating CD8+ T cells and their secreted factor GZMK as an upstream mechanism that induced age-related changes in the brain vasculature and subsequently led to synaptic alterations and cognitive decline.

Taken together with this rapidly growing body of work, our data advanced complementary strategies to rejuvenate cognition in old age by either targeting the trafficking of infiltrating CD8+ T cells into distinct regions of the aged brain or systemically inhibiting age-associated CD8+ T cell-derived factors such as GZMK in the blood circulation. More broadly, age-related changes in circulating CD8+ T cells are linked to multimorbidity and premature senescence in a variety of peripheral tissues,[52] which pose an important therapeutic target for broad age-associated disorders that extend beyond deficits in neurological functions.

Limitations of the study

The field of brain-body communication shows that the effects of young and old blood are driven by multitudinous peripheral factors that work in concert to drive the full effects of aging. In this context, the aim of our study was to identify age-specific factors that contribute to CD8+ T cell-driven cognitive decline, specifically in aging. As such, our data builds on this emerging body of work that targeting a single factor in circulation through a pharmacological approach is sufficient to promote functional recovery at old age. While we acknowledge mechanistic limitations in this pharmacological approach, such as a lack of cell specificity, our focus on a pharmacological GZMK inhibitor approach was prompted by the emphasis on the translational potential of our research.

While our work suggested that age-associated CD8+ T cells were sufficient to promote cognitive impairments, in part through GZMK, we note that we did not investigate whether other peripheral CD8+ T cell populations promote age-related cognitive decline. Additionally, while increased GZMK is a hallmark of age-associated CD8+ T cells, innate-like lymphocytes and natural killer (NK) cells express GZMK.[53,54] Notwithstanding, by functionally demonstrating the effect of CD8+ T cell-derived GZMK, we provided a proof of concept for the role of peripheral CD8+ T cells in age-related cognitive decline. Mechanistically, our transcriptomics data posited interactions between aged CD8+ T cells and their secreted factor, GZMK, and brain-barrier cells as a potential mechanism by which circulating aged CD8+ T cells impacted the aged hippocampus to promote cognitive decline. However, which barrier cells are involved in this process, as well as the molecular mechanisms downstream of GZMK on the vasculature, are unknown. Last, we highlighted that the effects of aged circulating CD8+ T cells were likely the result of multiple pro-aging secreted factors and anticipate that our findings will prompt further mechanistic investigations identifying aged CD8+ T cell-derived pro-aging circulating factors.

RESOURCE AVAILABILITY

Lead contact

Further information and requests for resources and reagents should be directed to and will be fulfilled by the lead contact, Dr. Saul Villeda (saul.villeda@ucsf.edu).

Materials availability

The plasmids generated in this study are available upon request.

Data and code availability

- All single-cell, single-nucleus, and bulk RNA-seq data have been deposited in the Gene Expression Omnibus (GEO) and are publicly available as of the date of publication. The accession numbers are listed in the key resources table.
- This paper does not report any original code.
- Any additional information required to reanalyze the data reported in this paper is available from the lead contact upon request.

ACKNOWLEDGMENTS

We thank Dr. Ari Molofsky and Dr. Zhaoqing Ding for critically reading the manuscript. This work was funded by the Simons Foundation (S.A.V.), the Bakar Family Foundation (S.A.V.), the National Science Foundation (J.S.), Impetus (J.S.), the Hillblom Foundation (G.B.), a Frontiers in Medical Research fellowship (K.J.B.P.), the Hevolution Foundation (S.A.V.), the American Federation for Aging Research (T.A.), the Multiple Sclerosis Foundation (A.P.), a gift from Marc and Lynne Benioff, and the National Institute on Aging (AG086042 [J.S.], AG081038 [G.B.], AG064823 [A.B.S.], and AG077816 [S.A.V.]). We acknowledge the UCSF Parnassus Flow Core (RRID: SCR_018206) and support from a DRC Center Grant NIH P30 DK063720 for assistance with flow cytometry. We thank the Genomics Core at the UCSF Institute for Human Genetics for assistance with CITE-seq and snRNA-seq.

AUTHOR CONTRIBUTIONS

J.S. and S.A.V. developed the concept and designed the experiments. J.S. collected and analyzed data. J.S. performed molecular, biochemical, and *in vivo* studies and behavioral analyses. G.B., K.J.B.P., T.A., A.R.P., L.R.,

R.C., C.E.S., Z.J.H., and A.B.S. assisted with molecular, biochemical, and *in vivo* studies. J.C. assisted with RNA-seq analysis. J.S. and G.B. generated the schematics. J.S. and S.A.V. wrote the manuscript. S.A.V. supervised all aspects of this project. All authors had the opportunity to discuss results and comment on the manuscript.

DECLARATION OF INTERESTS

S.A.V. is a co-founder of Ceiba Bio, Inc. and consulted for The Herrick Company, Inc.

STAR★METHODS

Detailed methods are provided in the online version of this paper and include the following:

- KEY RESOURCES TABLE
- EXPERIMENTAL MODEL AND SUBJECT DETAILS
  - Mouse strains
- METHOD DETAILS
  - Tissue collection
  - Lymphocyte isolation
  - Parabiosis
  - CD8a Antibody Depletion
  - GZMK inhibition
  - Adoptive transfer of CD8+ T cells
  - CITE-seq
  - Single nucleus RNA sequencing
  - Single cell and single nucleus RNA sequencing analysis
  - Bulk RNA isolation and sequencing
  - Flow Cytometry
  - RT-qPCR analysis
  - Immunohistochemistry
  - Western Blot Analysis
  - Cell Culture
  - GZMK ELISA
  - HDTVI
  - Retrovirus production
  - NOR
  - RAWM
  - Y maze
  - Fear conditioning
- QUANTIFICATION AND STATISTICAL ANALYSIS
  - Data, statistical analyses, and reproducibility

SUPPLEMENTAL INFORMATION

Supplemental information can be found online at https://doi.org/10.1016/j.immuni.2026.04.014.

Received: July 21, 2024
Revised: October 27, 2025
Accepted: April 20, 2026

REFERENCES

1. Hou, Y., Dan, X., Babbar, M., Wei, Y., Hasselbalch, S.G., Croteau, D.L., and Bohr, V.A. (2019). Ageing as a risk factor for neurodegenerative disease. Nat. Rev. Neurol. *15*, 565–581. https://doi.org/10.1038/s41582-019-0244-7.
2. Villeda, S.A., Luo, J., Mosher, K.I., Zou, B., Britschgi, M., Bieri, G., Stan, T.M., Fainberg, N., Ding, Z., Eggel, A., et al. (2011). The ageing systemic milieu negatively regulates neurogenesis and cognitive function. Nature *477*, 90–94. https://doi.org/10.1038/nature10357.
3. Yousef, H., Czupalla, C.J., Lee, D., Chen, M.B., Burke, A.N., Zera, K.A., Zandstra, J., Berber, E., Lehallier, B., Mathur, V., et al. (2019). Aged blood impairs hippocampal neural precursor activity and activates microglia via brain endothelial cell VCAM1. Nat. Med. *25*, 988–1000. https://doi.org/10.1038/s41591-019-0440-4.
4. Rodrigues, L.P., Teixeira, V.R., Alencar-Silva, T., Simonassi-Paiva, B., Pereira, R.W., Pogue, R., and Carvalho, J.L. (2021). Hallmarks of aging and immunosenescence: Connecting the dots. Cytokine Growth Factor Rev. *59*, 9–21. https://doi.org/10.1016/j.cytogfr.2021.01.006.
5. Franceschi, C., Garagnani, P., Parini, P., Giuliani, C., and Santoro, A. (2018). Inflammaging: a new immune–metabolic viewpoint for age-related diseases. Nat. Rev. Endocrinol. *14*, 576–590. https://doi.org/10.1038/s41574-018-0059-4.
6. Fulop, T., Larbi, A., Dupuis, G., Le Page, A.L., Frost, E.H., Cohen, A.A., Witkowski, J.M., and Franceschi, C. (2018). Immunosenescence and Inflamm-Aging As Two Sides of the Same Coin: Friends or Foes? Front. Immunol. *8*, 1960. https://doi.org/10.3389/fimmu.2017.01960.
7. Baruch, K., Ron-Harel, N., Gal, H., Deczkowska, A., Shifrut, E., Ndifon, W., Mirlas-Neisberg, N., Cardon, M., Vaknin, I., Cahalon, L., et al. (2013). CNS-specific immunity at the choroid plexus shifts toward destructive Th2 inflammation in brain aging. Proc. Natl. Acad. Sci. USA. *110*, 2264–2269. https://doi.org/10.1073/pnas.1211270110.
8. Smith, L.K., He, Y., Park, J.-S., Bieri, G., Snethlage, C.E., Lin, K., Gontier, G., Wabl, R., Plambeck, K.E., Udeochu, J., et al. (2015). β2-microglobulin is a systemic pro-aging factor that impairs cognitive function and neurogenesis. Nat. Med. *21*, 932–937. https://doi.org/10.1038/nm.3898.
9. Dulken, B.W., Buckley, M.T., Navarro Negredo, P.N., Saligrama, N., Cayrol, R., Leeman, D.S., George, B.M., Boutet, S.C., Hebestreit, K., Pluvinage, J.V., et al. (2019). Single-cell analysis reveals T cell infiltration in old neurogenic niches. Nature *571*, 205–210. https://doi.org/10.1038/s41586-019-1362-5.
10. Jin, W.-N., Shi, K., He, W., Sun, J.-H., Van Kaer, L.V., Shi, F.-D., and Liu, Q. (2021). Neuroblast senescence in the aged brain augments natural killer cell cytotoxicity leading to impaired neurogenesis and cognition. Nat. Neurosci. *24*, 61–73. https://doi.org/10.1038/s41593-020-00745-w.
11. Minhas, P.S., Latif-Hernandez, A., McReynolds, M.R., Durairaj, A.S., Wang, Q., Rubin, A., Joshi, A.U., He, J.Q., Gauba, E., Liu, L., et al. (2021). Restoring metabolism of myeloid cells reverses cognitive decline in ageing. Nature *590*, 122–128. https://doi.org/10.1038/s41586-020-03160-0.
12. Groh, J., Knöpper, K., Arampatzi, P., Yuan, X., Lößlein, L., Saliba, A.-E., Kastenmüller, W., and Martini, R. (2021). Accumulation of cytotoxic T cells in the aged CNS leads to axon degeneration and contributes to cognitive and motor decline. Nat. Aging *1*, 357–367. https://doi.org/10.1038/s43587-021-00049-z.
13. Kaya, T., Mattugini, N., Liu, L., Ji, H., Cantuti-Castelvetri, L., Wu, J., Schifferer, M., Groh, J., Martini, R., Besson-Girard, S., et al. (2022). CD8+ T cells induce interferon-responsive oligodendrocytes and microglia in white matter aging. Nat. Neurosci. *25*, 1446–1457. https://doi.org/10.1038/s41593-022-01183-6.
14. Schroer, A.B., Ventura, P.B., Sucharov, J., Misra, R., Chui, M.K.K., Bieri, G., Horowitz, A.M., Smith, L.K., Encabo, K., Tenggara, I., et al. (2023). Platelet factors attenuate inflammation and rescue cognition in ageing. Nature *620*, 1071–1079. https://doi.org/10.1038/s41586-023-06436-3.
15. Smith, L.K., Verovskaya, E., Bieri, G., Horowitz, A.M., von von Ungern-Sternberg, S.N.I., Lin, K., Seizer, P., Passegué, E., and Villeda, S.A. (2020). The aged hematopoietic system promotes hippocampal-dependent cognitive decline. Aging Cell *19*, e13192. https://doi.org/10.1111/acel.13192.
16. Mogilenko, D.A., Shpynov, O., Andhey, P.S., Arthur, L., Swain, A., Esaulova, E., Brioschi, S., Shchukina, I., Kerndl, M., Bambouskova, M., et al. (2021). Comprehensive Profiling of an Aging Immune System Reveals Clonal GZMK+ CD8+ T Cells as Conserved Hallmark of Inflammaging. Immunity *54*, 99–115.e12. https://doi.org/10.1016/j.immuni.2020.11.005.
17. Han, S., Georgiev, P., Ringel, A.E., Sharpe, A.H., and Haigis, M.C. (2023). Age-associated remodeling of T cell immunity and metabolism. Cell Metab. *35*, 36–55. https://doi.org/10.1016/j.cmet.2022.11.005.

18. Unger, M.S., Li, E., Scharnagl, L., Poupardin, R., Altendorfer, B., Mrowetz, H., Hutter-Paier, B., Weiger, T.M., Heneka, M.T., Attems, J., et al. (2020). CD8+ T-cells infiltrate Alzheimer's disease brains and regulate neuronal- and synapse-related gene expression in APP-PS1 transgenic mice. Brain Behav. Immun. *89*, 67–86. https://doi.org/10.1016/j.bbi.2020.05.070.

19. Altendorfer, B., Unger, M.S., Poupardin, R., Hoog, A., Asslaber, D., Gratz, I.K., Mrowetz, H., Benedetti, A., de de Sousa, D.M.B., Greil, R., et al. (2022). Transcriptomic Profiling Identifies CD8+ T Cells in the Brain of Aged and Alzheimer's Disease Transgenic Mice as Tissue-Resident Memory T Cells. J. Immunol. *209*, 1272–1285. https://doi.org/10.4049/jimmunol.2100737.

20. Moreno-Valladares, M., Moreno-Cugnon, L., Silva, T.M., Garcés, J.P., Saenz-Antoñanzas, A., Álvarez-Satta, M., and Matheu, A. (2020). CD8+ T cells are increased in the subventricular zone with physiological and pathological aging. Aging Cell *19*, e13198. https://doi.org/10.1111/acel.13198.

21. Katsimpardi, L., Litterman, N.K., Schein, P.A., Miller, C.M., Loffredo, F.S., Wojtkiewicz, G.R., Chen, J.W., Lee, R.T., Wagers, A.J., and Rubin, L.L. (2014). Vascular and Neurogenic Rejuvenation of the Aging Mouse Brain by Young Systemic Factors. Science *344*, 630–634. https://doi.org/10.1126/science.1251141.

22. Ho, T.T., Dellorusso, P.V., Verovskaya, E.V., Bakker, S.T., Flach, J., Smith, L.K., Ventura, P.B., Lansinger, O.M., Hérault, A., Zhang, S.Y., et al. (2021). Aged hematopoietic stem cells are refractory to bloodborne systemic rejuvenation interventions. J. Exp. Med. *218*, e20210223. https://doi.org/10.1084/jem.20210223.

23. Cyster, J.G., and Goodnow, C.C. (1995). Pertussis toxin inhibits migration of B and T lymphocytes into splenic white pulp cords. J. Exp. Med. *182*, 581–586. https://doi.org/10.1084/jem.182.2.581.

24. Klonowski, K.D., Williams, K.J., Marzo, A.L., Blair, D.A., Lingenheld, E.G., and Lefrançois, L. (2004). Dynamics of Blood-Borne CD8 Memory T Cell Migration In Vivo. Immunity *20*, 551–562. https://doi.org/10.1016/s1074-7613(04)00103-7.

25. Allen Institute for Brain Science. (2011).Allen Mouse Brain. Atlas [dataset]. Allen Institute for Brain Science. mouse.brain-map.org.

26. Van Kaer, L.V., Ashton-Rickardt, P.G., Ploegh, H.L., and Tonegawa, S. (1992). TAP1 mutant mice are deficient in antigen presentation, surface class I molecules, and CD4−8+ T cells. Cell *71*, 1205–1214. https://doi.org/10.1016/s0092-8674(05)80068-6.

27. Lan, F., Li, J., Miao, W., Sun, F., Duan, S., Song, Y., Yao, J., Wang, X., Wang, C., Liu, X., et al. (2025). GZMK-expressing CD8+ T cells promote recurrent airway inflammatory diseases. Nature *638*, 490–498. https://doi.org/10.1038/s41586-024-08395-9.

28. Turner, C.T. (2025). Pro-inflammatory granzyme K contributes extracellularly to disease. Front. Immunol. *16*, 1620670. https://doi.org/10.3389/fimmu.2025.1620670.

29. Schwinn, M.K., Machleidt, T., Zimmerman, K., Eggers, C.T., Dixon, A.S., Hurst, R., Hall, M.P., Encell, L.P., Binkowski, B.F., and Wood, K.V. (2018). CRISPR-Mediated Tagging of Endogenous Proteins with a Luminescent Peptide. ACS Chem. Biol. *13*, 467–474. https://doi.org/10.1021/acschembio.7b00549.

30. Horowitz, A.M., Fan, X., Bieri, G., Smith, L.K., Sanchez-Diaz, C.I., Schroer, A.B., Gontier, G., Casaletto, K.B., Kramer, J.H., Williams, K.E., et al. (2020). Blood factors transfer beneficial effects of exercise on neurogenesis and cognition to the aged brain. Science *369*, 167–173. https://doi.org/10.1126/science.aaw2622.

31. Richardson, K.C., Aubert, A., Turner, C.T., Nabai, L., Hiroyasu, S., Pawluk, M.A., Cederberg, R.A., Zhao, H., Jung, K., Burleigh, A., et al. (2024). Granzyme K mediates IL-23-dependent inflammation and keratinocyte proliferation in psoriasis. Front. Immunol. *15*, 1398120. https://doi.org/10.3389/fimmu.2024.1398120.

32. Turner, C.T., Zeglinski, M.R., Richardson, K.C., Zhao, H., Shen, Y., Papp, A., Bird, P.I., and Granville, D.J. (2019). Granzyme K Expressed by Classically Activated Macrophages Contributes to Inflammation and Impaired Remodeling. J. Investig. Dermatol. *139*, 930–939. https://doi.org/10.1016/j.jid.2018.09.031.

33. Bieri, G., Schroer, A.B., and Villeda, S.A. (2023). Blood-to-brain communication in aging and rejuvenation. Nat. Neurosci. *26*, 379–393. https://doi.org/10.1038/s41593-022-01238-8.

34. Ruiz-Fernández, I., Sánchez-Díaz, R., Ortega-Sollero, E., and Martín, P. (2024). Update on the role of T cells in cognitive impairment. Br. J. Pharmacol. *181*, 799–815. https://doi.org/10.1111/bph.16214.

35. Negredo, P.N., and Brunet, A. (2021). Unwanted help from T cells in the aging central nervous system. Nat. Aging *1*, 330–331. https://doi.org/10.1038/s43587-021-00053-3.

36. Liston, A., and Yshii, L. (2023). T cells drive aging of the brain. Nat. Immunol. *24*, 12–13. https://doi.org/10.1038/s41590-022-01390-0.

37. Hu, D., and Weiner, H.L. (2024). Unraveling the dual nature of brain CD8+ T cells in Alzheimer's disease. Mol. Neurodegener. *19*, 16. https://doi.org/10.1186/s13024-024-00706-y.

38. Su, W., Saravia, J., Risch, I., Rankin, S., Guy, C., Chapman, N.M., Shi, H., Sun, Y., Kc, A., Li, W., et al. (2023). CXCR6 orchestrates brain CD8+ T cell residency and limits mouse Alzheimer's disease pathology. Nat. Immunol. *24*, 1735–1747. https://doi.org/10.1038/s41590-023-01604-z.

39. Chen, X., Firulyova, M., Manis, M., Herz, J., Smirnov, I., Aladyeva, E., Wang, C., Bao, X., Finn, M.B., Hu, H., et al. (2023). Microglia-mediated T cell infiltration drives neurodegeneration in tauopathy. Nature *615*, 668–677. https://doi.org/10.1038/s41586-023-05788-0.

40. Terrabuio, E., Pietronigro, E.C., Bani, A., Della Bianca, V., Laudanna, C., Rossi, B., Finotti, G., Santos-Lima, B., Zenaro, E., Turano, E., et al. (2025). CD103–CD8+ T cells promote neurotoxic inflammation in Alzheimer's disease via granzyme K–PAR-1 signaling. Nat. Commun. *16*, 8372. https://doi.org/10.1038/s41467-025-62405-6.

41. Mason, H.D., Latour, Y.L., Boughter, C.T., Johnson, K.R., Maric, D., Dorrier, C.E., Guedes, V.A., Lai, C., Duncker, P.C., Johnson, A.M., et al. (2025). Granzyme K+ CD8 T cells slow tauopathy progression by targeting microglia. Nat. Immunol. *26*, 1152–1167. https://doi.org/10.1038/s41590-025-02198-4.

42. Rustenhoven, J., Drieu, A., Mamuladze, T., de de Lima, K.A., Dykstra, T., Wall, M., Papadopoulos, Z., Kanamori, M., Salvador, A.F., Baker, W., et al. (2021). Functional characterization of the dural sinuses as a neuroimmune interface. Cell *184*, 1000–1016.e27. https://doi.org/10.1016/j.cell.2020.12.040.

43. Piehl, N., van van Olst, L., Ramakrishnan, A., Teregulova, V., Simonton, B., Zhang, Z., Tapp, E., Channappa, D., Oh, H., Losada, P.M., et al. (2022). Cerebrospinal fluid immune dysregulation during healthy brain aging and cognitive impairment. Cell *185*, 5028–5039.e13. https://doi.org/10.1016/j.cell.2022.11.019.

44. Flemming, A. (2021). GZMK+ T cells a hallmark of immune ageing. Nat. Rev. Immunol. *21*, 1. https://doi.org/10.1038/s41577-020-00486-8.

45. Gao, Y., Liu, R., Shi, J., Shan, W., Zhou, H., Chen, Z., Yue, X., Zhang, J., Luo, Y., Pan, W., et al. (2025). Clonal GZMK+CD8+ T cells are identified as a hallmark of the pathogenesis of cGVHD-induced bronchiolitis obliterans syndrome after allogeneic hematopoietic stem cell transplantation. EBiomedicine *112*, 105535. https://doi.org/10.1016/j.ebiom.2024.105535.

46. Simon, M.M., Kramer, M.D., Prester, M., and Gay, S. (1991). Mouse T-cell associated serine proteinase 1 degrades collagen type IV: a structural basis for the migration of lymphocytes through vascular basement membranes. Immunology *73*, 117–119.

47. Guo, C.-L., Wang, C.-S., Wang, Z.-C., Liu, F.-F., Liu, L., Yang, Y., Li, X., Guo, B., Lu, R.-Y., Liao, B., et al. (2024). Granzyme K+CD8+ T cells interact with fibroblasts to promote neutrophilic inflammation in nasal polyps. Nat. Commun. *15*, 10413. https://doi.org/10.1038/s41467-024-54685-1.

48. Turner, C.T., Zeglinski, M.R., Boivin, W., Zhao, H., Pawluk, M.A., Richardson, K.C., Chandrabalan, A., Bird, P., Ramachandran, R., Sehmi, R., et al. (2023). Granzyme K contributes to endothelial microvascular damage and leakage during skin inflammation. Br. J. Dermatol. *189*, 279–291. https://doi.org/10.1093/bjd/ljac017.

49. Bieri, G., Pratt, K.J.B., Fuseya, Y., Aghayev, T., Sucharov, J., Horowitz, A.M., Philp, A.R., Fonseca-Valencia, K., Chu, R., Phan, M., et al. (2026). Liver exerkine reverses aging- and Alzheimer's-related memory loss via vasculature. Cell *189*, 1499–1516.e25. https://doi.org/10.1016/j.cell.2026.01.024.

50. Shi, S.M., Suh, R.J., Shon, D.J., Garcia, F.J., Buff, J.K., Atkins, M., Li, L., Lu, N., Sun, B., Luo, J., et al. (2025). Glycocalyx dysregulation impairs blood–brain barrier in ageing and disease. Nature *639*, 985–994. https://doi.org/10.1038/s41586-025-08589-9.

51. Park, M.H., Lee, J.Y., Park, K.H., Jung, I.K., Kim, K.-T., Lee, Y.-S., Ryu, H.-H., Jeong, Y., Kang, M., Schwaninger, M., et al. (2018). Vascular and Neurogenic Rejuvenation in Aging Mice by Modulation of ASM. Neuron *100*, 167–182.e9. https://doi.org/10.1016/j.neuron.2018.09.010.

52. Desdín-Micó, G., Soto-Heredero, G., Aranda, J.F., Oller, J., Carrasco, E., Gabandé-Rodríguez, E., Blanco, E.M., Alfranca, A., Cussó, L., Desco, M., et al. (2020). T cells with dysfunctional mitochondria induce multimorbidity and premature senescence. Science *368*, 1371–1376. https://doi.org/10.1126/science.aax0860.

53. Kim, H.-Y., and Ha, H. (2024). Distinct granzyme k expression in immune cells: a single-cell rna-seq meta-analysis. Genes Genomics *46*, 1097–1106. https://doi.org/10.1007/s13258-024-01555-1.

54. Duquette, D., Harmon, C., Zaborowski, A., Michelet, X., O'Farrelly, C., Winter, D., Koay, H.-F., and Lynch, L. (2023). Human Granzyme K Is a Feature of Innate T Cells in Blood, Tissues, and Tumors, Responding to Cytokines Rather than TCR Stimulation. J. Immunol. *211*, 633–647. https://doi.org/10.4049/jimmunol.2300083.

55. Villeda, S.A., Plambeck, K.E., Middeldorp, J., Castellano, J.M., Mosher, K.I., Luo, J., Smith, L.K., Bieri, G., Lin, K., Berdnik, D., et al. (2014). Young blood reverses age-related impairments in cognitive function and synaptic plasticity in mice. Nat. Med. *20*, 659–663. https://doi.org/10.1038/nm.3569.

56. Gontier, G., Iyer, M., Shea, J.M., Bieri, G., Wheatley, E.G., Ramalho-Santos, M., and Villeda, S.A. (2018). Tet2 Rescues Age-Related Regenerative Decline and Enhances Cognitive Function in the Adult Mouse Brain. Cell Rep. *22*, 1974–1981. https://doi.org/10.1016/j.celrep.2018.02.001.

57. Stoeckius, M., Hafemeister, C., Stephenson, W., Houck-Loomis, B., Chattopadhyay, P.K., Swerdlow, H., Satija, R., and Smibert, P. (2017). Simultaneous epitope and transcriptome measurement in single cells. Nat. Methods *14*, 865–868. https://doi.org/10.1038/nmeth.4380.

58. Lein, E.S., Hawrylycz, M.J., Ao, N., Ayres, M., Bensinger, A., Bernard, A., Boe, A.F., Boguski, M.S., Brockway, K.S., Byrnes, E.J., et al. (2007). Genome-wide atlas of gene expression in the adult mouse brain. Nature *445*, 168–176. https://doi.org/10.1038/nature05453.

59. Liu, Z., Gu, Y., Shin, A., Zhang, S., and Ginhoux, F. (2020). Analysis of Myeloid Cells in Mouse Tissues with Flow Cytometry. Star Protoc. *1*, 100029. https://doi.org/10.1016/j.xpro.2020.100029.

60. Stevenson, M.E., Bieri, G., Kaletsky, R., St Ange, J.St., Remesal, L., Pratt, K.J.B., Zhou, S., Weng, Y., Murphy, C.T., and Villeda, S.A. (2023). Neuronal activation of Gαq EGL-30/GNAQ late in life rejuvenates cognition across species. Cell Rep. *42*, 113151. https://doi.org/10.1016/j.celrep.2023.113151.

61. Kovacsics, D., and Raper, J. (2014). Transient Expression of Proteins by Hydrodynamic Gene Delivery in Mice. J. Vis. Exp. *87*, 51481. https://doi.org/10.3791/51481.

62. Alamed, J., Wilcock, D.M., Diamond, D.M., Gordon, M.N., and Morgan, D. (2006). Two-day radial-arm water maze learning and memory task; robust resolution of amyloid-related memory deficits in transgenic mice. Nat. Protoc. *1*, 1671–1679. https://doi.org/10.1038/nprot.2006.275.

Please cite this article in press as: Sucharov et al., Aged circulating CD8+ T cells and their secreted factors drive cognitive decline, Immunity (2026), https://doi.org/10.1016/j.immuni.2026.04.014

STAR★METHODS

KEY RESOURCES TABLE

REAGENT or RESOURCE	SOURCE	IDENTIFIER
Antibodies		
InVivoMAb anti-mouse CD8a (2.43)	BioXCell	Cat#BE0061; RRID: AB_1125541
InVivoMAb rat IgG2b (LTF-2)	BioXCell	Cat#BE0090; RRID: AB_1107780
InVivoMAb anti-mouse/human VLA-4 (CD49d)	BioXCell	Cat#BE0071; RRID: AB_1107657
GhostDye UV 450	Tonbo	Cat#13-0868
CD45-BV711	BD Biosciences	Cat#563709; RRID: AB_2687455
CD45-PE	Thermo Fisher	Cat#12-0451-82; RRID: AB_465668
CD45.2-FITC	eBioscience	Cat#11-0454-82; RRID: AB_465061
CD45.1-PE	eBioscience	Cat#12-0453-83; RRID: AB_465676
CD3-APC	Tonbo Biosciences	Cat#20-0031; RRID: AB_2621537
CD8a-PB	Thermo Fisher	Cat#MCD0828; RRID: AB_1488087
CD4-PE-Cyanine7	Thermo Fisher	Cat#25-0041-82; RRID: AB_469576
CD44-APC-eFluor 780	Thermo Fisher	Cat#47-0441-82; RRID: AB_1272244
CD69-AF700	Thermo Fisher	Cat#56-0691-82; RRID: AB_2815240
CD62L-PerCP-Cyanine5.5	Thermo Fisher	Cat#45-0621-82; RRID: AB_996667
GZMK-FITC	LSBio	Cat#C119554; RRID: AB_10799039
CCL5-PE-Cyanine7	BioLegend	Cat#149105; RRID: AB_2832528
IBA1	Wako	Cat#01919741; RRID: AB_839504
IBA1	Synaptic Systems	Cat#234-004; RRID: AB_2493179
CD68 (FA-11)	Bio-Rad	Cat#MCA1957T; RRID: AB_2074849
cFos (96F)	Cell Signaling	Cat#2250; RRID: AB_2247211
CD31	R&D	Cat#AF3628; RRID: AB_2161028
CD8 (4SM15)	eBioscience	Cat#14-0808-82; RRID: AB_2572861
Collagen1	Abcam	Cat#ab21286; RRID: AB_446161
ACTA2	Thermo Fisher	Cat#14-9760-82; RRID: AB_2572996
PAR1	Invitrogen	Cat#PA5-116040; RRID: AB_2900674
GAPDH	Abcam	Cat#ab8245; RRID: AB_2107448
beta-Tubulin	Eurogentec	Cat#MMS-435P; RRID: AB_2315514
Synapsin1	Abcam	Cat#ab18814; RRID: AB_444679
NR2A	Sigma Millipore	Cat#07-632; RRID: AB_310837
NR2B	Abcam	Cat#ab65783; RRID: AB_1658870
PSD95	Cell Signaling	Cat#2507; RRID: AB_561221
Homer1	Invitrogen	Cat#PA5-21487; RRID: AB_11155843
ZO1 (TJP1)	Thermo Fisher	Cat#40-2200; RRID: AB_2533456
Bacterial and virus strains		
NEB® 5-alpha Competent E. coli	New England Biolabs (NEB)	Cat#C2987U
Biological samples		
Mouse brain tissue	This paper	N/A
Mouse spleen tissue	This paper	N/A
Mouse plasma	This paper	N/A
Mouse T cells	This paper	N/A
Mouse brain endothelial cells	This paper	N/A
Chemicals, peptides, and recombinant proteins		
Ficoll-Paque	Cytiva	Cat#17144002
D-Pro-Phe-Arg-Chloromethylketone	MedChemExpress	Cat#HY-P4245

(*Continued on next page*)

Please cite this article in press as: Sucharov et al., Aged circulating CD8+ T cells and their secreted factors drive cognitive decline, Immunity (2026), https://doi.org/10.1016/j.immuni.2026.04.014

Continued

REAGENT or RESOURCE	SOURCE	IDENTIFIER
Hoechst 33342	Thermo Fisher	Cat#H3570
Pertussis Toxin	Thermo Fisher	Cat# PHZ1174
IL-2	Thermo Fisher	Cat#212-12
Tofacitinib	Selleckchem	Cat#S5001
BD Horizon™ Brilliant Stain Buffer	BD Biosciences	Cat#56379
Foxp3 / Transcription Factor Staining Buffer Set	eBiosciences	Cat# 00-5523-00
RIPA lysis buffer	Abcam	Cat#ab156034
Complete protease inhibitor	Sigma-Aldrich	Cat#4693116001
Phosphatase inhibitor	Thermo Fisher	Cat#78420
Ficoll-Paque	Cytiva	Cat#17144002
GolgiStop Protein Transport Inhibitor	BD	Cat#554724
TrueBlack	Biotium	Cat#23007
Critical commercial assays		
Direct-zol™ RNA Purification Kit, Miniprep Plus	Zymo Research	Cat#R2072
High Capacity cDNA Reverse Transcription kit	Thermo Fisher	Cat#4374966
NEBuilder HiFi DNA Assembly Kit	NEB	Cat#E5520S
PowerUp SYBR Green Master Mix	Thermo Fisher	Cat#A25742
Miltenyi Neural Dissociation Kits (P)	Miltenyi	Cat#130-092-628
CD8a+ T cell Isolation Kit	Miltenyi Biotech	Cat#130-104-075
Dynabeads™ Protein G Immunoprecipitation Kit	Thermo Fisher	Cat#10007D
GZMK ELISA	MyBioSource	Cat#MBS453082
Nano-Glo HiBiT Lytic Detection System	Promega	Cat#N3030
Mouse T-Activator CD3/CD28 beads	Gibco	Cat#11452D
Lenti-X concentrator	Takara	Cat#631232
Q5 Site-directed Mutagenesis kit	NEB	Cat#E0554S
Deposited data		
Single-nucleus RNA sequencing data	This paper	GSE266468
Bulk RNA sequencing data	This paper	GSE266454
CITE-seq RNA sequencing data	This paper	GSE266467
Experimental models: Organisms/strains		
C57BL/6J	The Jackson Laboratory	Strain#000664
C57BlL6/J NIA Aging mouse colony	NIA	N/A
B6.SJL-Ptprca Pepcb/BoyJ	The Jackson Laboratory	Strain#002014
C57BL/6-Tg(UBC-GFP)30Scha/J	The Jackson Laboratory	Strain#004353
B6;129S2-Tap1tm1Arp/J	The Jackson Laboratory	Strain#002458
Oligonucleotides		
Gapdh qPCR FWD: GGGTGTGAACCACGAGAAAT	This paper	N/A
Gapdh qPCR REV: ACTGTGGTCATGAGCCCTTC	This paper	N/A
C1qa qPCR FWD: GTGCCCGGCTTCTATTACTT	This paper	N/A
C1qa qPCR REV: CCCGGAGGAAGACTTGATAAAC	This paper	N/A
Nfkb qPCR FWD: GAAATTCCTGATCCAGACAAAAAC	This paper	N/A
Nfkb qPCR REV: ATCACTTCAATGGCCTCTGTGTAG	This paper	N/A
Cd11b qPCR FWD: TCCGGTAGCATCAACAACAT	This paper	N/A
Cd11b qPCR REV: GGTGAAGTGAATCCGGAACT	This paper	N/A
TNFa qPCR FWD: TTGGAGTCATTGCTCTGTGAA	This paper	N/A
TNFa qPCR REV: GGGTCAGAGTAAAGGGGTCAG	This paper	N/A
Il1b qPCR FWD: TGGCCTTGGGCCTCAAAGGAAAG	This paper	N/A
Il1b qPCR REV: TGCTTGGGATCCACACTCTCCAGC	This paper	N/A

(*Continued on next page*)

Please cite this article in press as: Sucharov et al., Aged circulating CD8+ T cells and their secreted factors drive cognitive decline, Immunity (2026), https://doi.org/10.1016/j.immuni.2026.04.014

Continued

REAGENT or RESOURCE	SOURCE	IDENTIFIER
Homer1 qPCR FWD: CTGCCTGAGTGTCGTGGAAG		N/A
Homer1 qPCR REV: ATGATTTCACTCGCGCTGAC	This paper	N/A
Recombinant DNA		
GZMK	OriGene	Cat#MR215106
CCL5	OriGene	Cat# MG227153
pTB CMV IRES eGFP	This paper	N/A
pTB CMV GZMK-HiBiT IRES eGFP	This paper	N/A
MSCV eGFP	This paper	N/A
MSCV GZMK	This paper	N/A
Software and algorithms		
FIJI/ImageJ2	ImageJ	https://imagej.net/software/fiji/
Prism 10	GraphPad	https://www.graphpad.com
Zeiss Zen 3.7/3.3	Zeiss	N/A
Cell Ranger version 7.1.0.	10X Genomics	https://support.10xgenomics.com/single-cell-gene-expression/software/downloads/latest
RStudio	Posit	https://posit.co/downloads/
Seurat v5	Satija Lab	https://satijalab.org/seurat/
Wheel Manager Software	MedAssociates	Cat# SOF-860
Smart Video Tracking Software	Panlab/Harvard Apparatus	http://www.panlab.com/en/products/smart-video-tracking-software-panlab
ChemiDoc Image Lab Software 6.1	BioRad	N/A
EthoVision XT	Noldus	N/A

EXPERIMENTAL MODEL AND SUBJECT DETAILS

Mouse strains

The following mouse lines were used: C57BL/6J mice (Jackson Laboratory line 000664), C57BL/6 aged mice (National Institutes of Aging), C57BL/6-Tg(UBC-GFP)30Scha/J mice (Jackson Laboratory line 004353), B6.SJL-Ptprca Pepcb/BoyJ mice (Jackson Laboratory line 002014), and B6;129S2-Tap1tm1Arp/J mice (Jackson Laboratory line 002458). All studies were done in young (4–5 month) or aged (22–24 month) male mice. The numbers of mice used to result in statistically significant differences were calculated using standard power calculations with a = 0.05 and a power of 0.8. We used an online tool to calculate power (https://www.stat.uiowa.edu/~rlenth/Power/index.html) and samples size based on experience with the respective tests, variability of the assays and inter-individual differences within groups. All other studies were performed with male mice. Mice were housed under specific pathogen-free conditions under a 12h light-dark cycle, and all animal handling and use was in accordance with institutional guidelines approved by the University of California, San Francisco Institutional Animal Care and Use Committee (IACUC) and the Stanford University Administrative Panel on Laboratory Animal Care (APLAC).

METHOD DETAILS

Tissue collection

Mice were anesthetized with 87.5 mg per kg ketamine and 12.5 mg per kg xylazine and transcardially perfused with ice-cold phosphate-buffered saline. To process the brains, the whole brain was sectioned in half along the sagittal plane. The hippocampus from one hemisphere was subdissected and snap-frozen and the other was fixed in phosphate-buffered 4% paraformaldehyde, pH 7.4 at 4 °C for 48 h before cryoprotection with 30% sucrose.

Lymphocyte isolation

For flow cytometry analysis, the hippocampus was subsidence, dissociated with the Neural Tissue Dissociation Kit (P) (Miltenyi Biotech) according to manufacturer instructions, then filtered through a 70 μm cell strainer and washed with 10 mL of MACS buffer (PBS with 2% FBS). For collection of splenocytes, spleens were removed, mechanically dissociated with a syringe plunger over a 70 μm cell strainer and washed with 10 ml of MACS. Cells were centrifuged and RBC lysis was performed (155 mM NH4Cl, 1 mM KHCO3 and 0.1 mM EDTA) with 2 ml for 5 minutes room temperature (RT). Subsequently, cells were washed, spun 500 RCF for 5 minutes, and resuspended in MACS. For lymph node isolation, cervical, axillary, brachial, and inguinal lymph nodes were removed and

Please cite this article in press as: Sucharov et al., Aged circulating CD8+ T cells and their secreted factors drive cognitive decline, Immunity (2026), https://doi.org/10.1016/j.immuni.2026.04.014

mechanically dissociated with a syringe plunger over a 70 μm cell strainer and washed with 10 mL of MACS. PBMCs were isolated from blood through RBC lysis (2 mL, 5 minutes RT) followed by washing with MACS and repeated lysis until sample was mainly colorless or with a 2:1 Ficoll gradient.

Parabiosis

Parabiosis surgery followed previously described procedures.[55,56] Pairs of C57BL/6J (22 months, aged) or B6.SJL-Ptprca Pepcb/BoyJ (3 months, young) mice were anaesthetized and prepared for surgery. Mirror-image incisions at the left and right flanks were made through the skin, and shorter incisions were made through the abdominal wall. The peritoneal openings of the adjacent parabionts were sutured together. Elbow and knee joints from each parabiont were sutured together, and the skin of each mouse was stapled (9-mm Autoclip, Clay Adams) to the skin of the adjacent parabiont. Each mouse was injected subcutaneously with enrofloxacin (Bayer) antibiotic, buprenorphine (Butler Schein), and carprofen (Rimadyl) as directed for pain and monitored during recovery. For overall health and maintenance behavior, recovery characteristics of paired weights and grooming were analyzed at various times after surgery. Parabionts were sacrificed 4 weeks after surgery.

CD8a Antibody Depletion

Aged (22–24 months) mice were treated i.p. with 200 μm of *InVivo*MAb anti-mouse CD8a (2.43, BioXCell, BE0061) or *InVivo*MAb rat IgG2b isotype control (LTF-2, BioXCell, BE0090) in 200 μL PBS every 4 days until time of sacrifice. Depletion of circulating $CD8^+$ T cells was confirmed with flow cytometry.

GZMK inhibition

Aged (22-24 months) mice were treated i.p. with 62.5 μg of GZMK inhibitor D-Pro-Phe-Arg-Chloromethylketone (MedChemExpress, HY-P4245) or saline control in 100 μL PBS every 4 days for a total of 4 injections, followed by behavioral testing.

Adoptive transfer of $CD8^+$ T cells

B6.SJL-Ptprca Pepcb/BoyJ (4 months) mice were treated i.p. with 200 μm of *InVivo*MAb anti-mouse CD8a in 200 μL PBS day -11 and -7 to deplete resident $CD8^+$ T cells. $CD8^+$ T cells were isolated from single cell suspensions of spleenocytes and PBMCs from young (3–4 months) or aged (22–28 months) C57BL/6J mice using the $CD8a^+$ T cell Isolation Kit (Miltenyi Biotech, 130-104-075) according to manufacturer instructions. For adoptive transfer of young or aged $CD8^+$ T cells, cells were immediately resuspended at concentrations of 3e5 (first injection) or 3e6 (second injection) in 100 μL saline and injected via tail vein. For pertussis toxin treatment (PTx) (Thermo Fisher Scientific, PHZ1174), cells were incubated at a concertation of 2e6 cells/mL in T cell Media (RPMI + 10% FBS + 1% p/s, NAA, L-glut, NaPyr + 50 μM BME) with IL-2 (1:2000, stock 1000 U/μL, Thermo Fisher, 212–12) and 0.5 μg/mL PTx or vehicle control. For tofacitinib (Selleckchem, S5001) and InVivoMAb anti-mouse/human VLA-4 (CD49d) (BioXCell, BE0071), cells were incubated at a concertation of 2e6 cells/mL in T cell Media (RPMI + 1.25% FBS + 1% p/s, NAA, L-glut, NaPyr + 50 μM BME) with IL-2 (1:2000, stock 1000 U/μL, Thermo Fisher, 212-12) and 10 μM Tofacitinib, 20 μg/mL anti-VLA-4, or vehicle (DMSO) control. Cells were incubated for 24 hours, then were washed three times with saline before resuspension at concentrations of 3e5 cells/100 μL saline (first injection) or 3e6 cells/100 μL saline (second injection) and injection via tail vein. Each mouse was injected i.v. with 100uL of cells in saline (3e5-3e6 cells/injection).

CITE-seq

CITE-seq analysis was performed on splenocytes isolated from four mice per group. Splenocytes were isolated as described above, blocked (2.4G2), then labeled with CD45.1 (A20, 1:200) and C45.2 (104, 1:200) antibodies in MACS for 30 minutes on ice. Samples were washed, then stained with a live/dead marker (Hoechst 33342, 1:10,000) before filtering through a 35 μm FACS tube filter sorting on a BD FACSAria Fusion with a 70 μm nozzle and with a flow rate of 1–2.5. Cells were first gated by forward and side scatter, then gated for doublets with height and width. 40,000 cells per sample that were Hoechst- and CD45.1+ or CD45.2+ were collected for sequencing analysis. Collected cells from each group were labeled with CITE-seq antibodies, as previously described.[57] Sorted cells were first blocked with TruStain fcX (BioLegend) for 10 min on ice, then stained with either CD8a or CD45 antibodies for sample separation during CITE-seq analysis. After 30 min of labelling, samples were washed three times then pooled into 6 groups (CD45.1+ young isochronic, CD45.1+ young heterochronic, CD45.2+ young heterochronic, CD45.1 + aged heterochronic, CD45.2+ aged heterochronic, and CD45.2+ aged isochronic). After combining grouped samples, the samples were incubated on ice with Total-seqB antibodies purchased from BioLegend. After 30 min of labelling, samples were washed three times before delivering the prepared samples to the UCSF-IHG Genomics Core for analysis with the 10x Genomics Chromium Single Cell Expression Solution 3′ kit with Feature Barcode Technology (v.3.1). The Genomics Core prepared cells for 10x Genomics Chromium single-cell capture. 25,000 cells were loaded per sample. cDNA libraries were prepared according to the standard 10x Genomics protocols. The final library pool was sequenced to a depth of 30,000 cDNA reads per cell and 3,000 ADT reads per cell on the NovaSeq X 10B system at the UCSF CAT Core. The raw base sequence calls were demultiplexed into sample-specific cDNA and ADT files with bcl2fastq/mkfastq sample sheet using Cell Ranger 7.1 (10x Genomics).

Please cite this article in press as: Sucharov et al., Aged circulating CD8+ T cells and their secreted factors drive cognitive decline, Immunity (2026), https://doi.org/10.1016/j.immuni.2026.04.014

CellPress
OPEN ACCESS

Single nucleus RNA sequencing

Neuronal nuclei were isolated based on the demonstrated protocol by 10x Genomics with modifications and performed on nuclei isolated from three mice per group. Briefly, flash-frozen dissected hippocampi were dounce homogenized (Wheaton, Cat# 357538) in 500μL of NP40 lysis buffer (10mM Tris-HCl (pH = 7.4), 10mM NaCl, 3mM MgCl2, 0.1% Nonidet P40 Substitute), 1mM DTT, 1x RNAse Inhibitor, Nuclease-free H2O) with 20 strokes of the loose pestle and 25 strokes of the tight pestle. 500 μL of NP40 lysis buffer was added and samples incubated for 7 minutes on ice. Samples were filtered through a 40 μm filter and centrifuged at 500 RCF for 5 min at 4°C. Samples were resuspended in 1ml of Wash Buffer (PBS, 1%BSA, 1xRNAse Inhibitor) and incubated for 5 min on ice. Samples were centrifuged at 500 RCF for 5 min at 4°C, supernatant was removed, and samples were resuspended in 400 uL of Wash Buffer with 1:10,000 dilution of Hoescht 33342 and incubated for five minutes before filtering through a 35μm FACS tube filter and sorting on a BD FACSAria II. Nuclei were sorted on a BD FACSAria Fusion with a 70 μm nozzle and with a flow rate of 1–2.5. Nuclei were first gated by forward and side scatter, then gated for doublets with height and width. Nuclei that were Hoechst+ were sorted and samples were combined per group. Isolated nuclei were given to the UCSF-IHG Genomics Core for analysis with the 10x Genomics Chromium Single Cell Expression Solution 3′ kit. The Genomics Core prepared cells for 10x Genomics Chromium single-cell capture. 30,000 nuclei were loaded per sample. cDNA libraries were prepared according to the standard 10x Genomics protocols. The final library pool was sequenced on the NovaSeq 6000 S2 system ($CD8^+$ depletion) or the NovaSeq X 10B system ($CD8^+$ adoptive transfer) at the UCSF CAT Core. The raw base sequence calls were demultiplexed into sample-specific cDNA files with bcl2fastq/mkfastq sample sheet using Cell Ranger 7.1 (10x Genomics). We note that due to technical limitations our sequencing approach did not capture robust numbers of astrocytes.

Single cell and single nucleus RNA sequencing analysis

Raw FASTQ files were processed and aligned to mm10 using the Cell Ranger software package (10x Genomics) for the RNA expression matrix, including introns in analysis for single nucleus analysis. Outputs from parabiosis CITE-seq and adoptive transfer snRNA-seq were integrated with Cell Ranger Aggr (10x Genomics) to normalize for sequencing depth. For parabiosis sequencing, a total of 59,846 cells were sequenced at a depth of 30,977 reads per cell and approximately a 68% sequencing saturation. For $CD8^+$ adoptive transfer sequencing, a total of 52,221 cells were sequenced at a depth of 37,013 reads per cell and approximately a 68% sequencing saturation of 34.1%. Further QC and analysis were performed on R 4.2.2. Lastly, for $CD8^+$ depletion sequencing, 15,237-16,194 cells were sequenced at a sequencing depth of 23,213 reads per cell and 37.6% sequencing saturation (IgG2b) or a sequencing depth of 32,910 reads per cell and 47.4% sequencing saturation (CD8a). Ambient RNA was removed with the SoupX package and data from the four samples was integrated using Seurat (2000 variable features, 1:20 dimensions). For all experiments, downstream analysis and data visualization was performed using Seurat, as well as packages DropletUtils, ggplot2, knitr, WriteXLS, RColorBrewer, data.table, stringr, ggplot2, forcats, dplyr, Nebulosa, and htmlwidgets. Data were processed to remove doublets and unwanted sources of variation by removing cells with more than 3,500 and fewer than 300 genes per cell or nuclei with more than 5,000 and fewer than 300 genes per cell and regressing on number of UMIs. Genes expressed in fewer than three cells or nuclei were filtered out. Cells with a percentage of mitochondrial genes of higher than 10% or nuclei with a percentage higher than 0.1% were removed. Final cell counts of 8341 (Young Iso), 8418 (Young Het 45.1), 9981 (Young Het 45.2), 5694 (Aged Het 45.1), 8480 (Aged Het 45.2), and 7364 (Aged Iso) and nuclei counts of 14,589 (Young CD8), 10,510 (Aged CD8), 24,463 (Ptx CD8), 12,079 (IgG2b), and 12,062 (CD8a) were used for gene expression analysis. The matrices of data were log-normalized in a sparse data matrix and PCA was applied to reduce dimensionality. The first 20 (parabiosis, CD8 depletion) or 30 (adoptive transfer) PCA components were used to cluster cells by Louvain clustering implemented in Seurat while UMAP plots were independently generated to aid in 2D representation of multi-dimensional data independent of the clustering. Cell types were identified using known markers, as well as the Allen Mouse Brain Atlas,[54,58] and clusters containing more than one cell type specific marker were excluded. Differential gene expression was performed with a minimum of 10% of cells or 5% nuclei expressed, log fold change threshold of 0.15, and a pseudocount of 0.1. Log-normalized gene expression data were used for visualizations with violin plots and UMAP feature plots. Average expression matrices were used for heatmap visualization. Volcano plots were created using the EnhancedVolcano package and UpSet plots with the ComplexHeatmap package. Pseudotime analysis was performed with monocle3. Predicted interactions were identified with CellChat.

Bulk RNA isolation and sequencing

RNA was isolated from previously flash frozen hippocampi from one hemisphere. Total RNA was isolated from samples by lysis using TRIzol Reagent (Thermo Fisher Scientific), separation with chloroform and precipitation with isopropyl alcohol, according to the manufacturer's instructions. Isolated RNA was sent to GENEWIZ for library construction and sequencing. Alignment of RNA-seq reads to the mouse mm10 transcriptome was performed using STAR using the ENCODE standard options, read counts were generated using RSEM and differential expression analysis was performed in R 3.6.1)\ using the DESeq2 package (detailed pipeline v.2.0.1 and options are available at GitHub (https://github.com/emc2cube/Bioinformatics/)). Genes significantly changed after treatment with were determined using a nominal $p<0.05$. GO term enrichment analysis was performed using PANTHER (v.18.0), with statistical enrichment-test over the Mus musculus reference genome (FDR<0.05). GO terms with fully overlapping genes were narrowed to one term. Heat maps were generated ggplot2. Module score analysis was performed by identifying cells expressing a dataset of z-scored differentially expressed genes ($p<0.05$) with the Seurat AddModuleScore function with a single nucleus RNA sequencing dataset.

Please cite this article in press as: Sucharov et al., Aged circulating CD8+ T cells and their secreted factors drive cognitive decline, Immunity (2026), https://doi.org/10.1016/j.immuni.2026.04.014

Flow Cytometry

Single cell suspensions of splenocytes, PBMCs, lymph nodes, and hippocampal cells were isolated as stated above, then approximately 1 × 10^6 cells per sample were stained on a round-bottom 96-well plate with a live/dead marker (GhostDye UV 450, Tonbo, 13-0868) 1:100 in PBS for 20 minutes RT. Cells were subsequently washed in FACS buffer (PBS with 2% FBS, 2 mM EDTA, 2mM NaN3) and spun for 2 minutes at 300 RCF. Samples were blocked with 2.4G2 (1:100 in FACS) for 10 minutes on ice. Cells were washed with FACS, then resuspended in an antibody cocktail in FACS buffer with Brilliant Stain Buffer (BD, 56379) at a 1:1 ratio for cell surface staining and incubated on ice for 30–60 minutes. After washing, cells were either fixed with 4% paraformaldehyde, washed and resuspended in FACS buffer for storage until analysis or followed with intracellular staining with the Foxp3 / Transcription Factor Staining Buffer Set (eBioscience, 00-5523-00) according to manufacturer instructions. Cells were analyzed using the BD LSR II Flow Cytometer at the UCSF Parnassus Flow Cytometry CoLab and Flow Jo software (TreeStar). Florescence minus one (FMO) controls were used for the initial antibody tests, then thereafter for certain stains. Immune cell populations after parabiosis were analyzed according to published protocols, with the same antibodies and concentrations used.[59] For T cell populations, antibodies used were as follows: CD45-BV711 (1:200, BD Biosciences, 563709), CD45-PE (1:200, ThermoFisher Scientific, 5010370), CD45.2-FITC (1:200, eBioscience, 11-0454-82), CD45.1-PE (1:200, eBioscience, 12-0453-83), CD3-APC (1:200, Tonbo Biosciences, 20-0031-U025), CD8a-PB (1:200, ThermoFisher Scientific, MCD0828), CD4-PE-Cyanine7 (1:200, ThermoFisher Scientific, 25-0041-82), CD44-APC-eFluor 780 (1:100, ThermoFisher Scientific, MCD0828), CD69-AF700 (1:100, ThermoFisher Scientific, 56-0691-82), CD62L-PerCP-Cyanine5.5 (1:100, ThermoFisher Scientific, 45-0621-82), GZMK-FITC (1:100, LSBio, LS-C692079-200), or CCL5-PE-Cyanine7 (1:100, BioLegend, 2308-03). For CD45-PE labeling injections, mice were injected i.v. with 200 ul of CD45-PE (1μ/100μL) in saline 3 minutes before sacrifice.

RT-qPCR analysis

To quantify mRNA expression, equal amounts of cDNA were synthesized using the High-Capacity cDNA Reverse Transcription kit (Thermo Fisher Scientific, 4368813), then mixed with SYBR Fast mix (Kapa Biosystems) and primers. *Gapdh* was amplified as an internal control. RT–qPCR was performed in the CFX384 Real Time System (Bio-Rad). Each sample and primer set were run in triplicates and relative expression was calculated using the 2-ΔΔct method.

Immunohistochemistry

Tissue processing and immunohistochemistry was performed on free-floating sections according to standard published techniques.[14,60] Cryoprotected brains were sectioned coronally at 40 μm with a cryomicrotome (Leica Camera). Free-floating coronal sections (40 μm) were permeabilized with pre-treatment buffer (0.2% TritonX-100 in TBST) for 30 minutes RT, then washed 3x with TBST and blocked with TBST + 5% NDS. Sections were then incubated overnight at 4 degrees C with anti-Iba1 (1:1,000, Wako, 01919741), anti-Iba1 (1:1000, Synaptic Systems, 234-004), anti-CD68 (1:250, FA-11, Bio-Rad, MCA1957t), anti-cFos (1:100, 96F, Cell Signaling, 2250), anti-CD31(1:200, R&D, AF3628), anti-CD8 (1:250, 4SM15, EBioscience, 14-0808-82), anti-Collagen1 (1:500, Abcam, ab21286), or anti-Acta2 (1:500, ThermoFisher Scientific, 14-9760-82), or anti-Par1 (1:200, Invitrogen, PA5-116040 in TBST + 5% NDS. Labelling was revealed using secondary antibodies at 1:500 in TBST + 3% NDS for 1 hour room temperature. Sections were imaged using confocal microscopy (Zeiss LSM800 or Zeiss LSM900) or bright-field microscopy (Keyance). Individual cell numbers and intensity in the dentate gyrus was quantified using ImageJ.

Western Blot Analysis

For Western blot analysis, samples were combined with RIPA lysis buffer (Abcam, ab156034) with complete protease inhibitor (4693116001, Sigma-Aldrich) and phosphatase inhibitor (Thermo Fisher Scientific, 78420). Subsequently, the samples were mixed with 4× NuPage LDS loading buffer (Invitrogen, NP0008), loaded onto an SDS polyacrylamide gel (Invitrogen) and transferred onto a nitrocellulose membrane. Equal loading of samples was confirmed using Ponceau S solution (Sigma-Aldrich, P7170) and membranes were imaged with the ChemiDoc System (Bio-Rad). The blots were blocked in 5% milk in Tris-buffered saline with Tween-20 and incubated with anti-GAPDH (6C5, 1:5,000, Abcam, ab8245), anti-beta-tubulin (1:1000, Eurogentec, MMS-435P-200), anti-Synapsin1 (1:250, Abcam, ab18814), anti-NR2A (1:1000, Sigma Millipore, 07–632), anti-NR2B (1:4000, Abcam, ab65783), anti-PSD95 (1:500, Cell Signaling, 2507S), anti-Homer1 (1:500, Invitrogen, PA5-21487), or anti-ZO1 (TJP1) (1:500, ThermoFisher Scientific, 40–2200). Horseradish-peroxidase-conjugated secondary antibodies (donkey anti-goat conjugated HRP (1:2,000, Invitrogen, A15999), goat anti-mouse conjugated HRP (1:2,000, Millipore, AP124P), and donkey anti-rabbit conjugated HRP (1:2,000, GE Healthcare, NA934V)) and an ECL kit (GE Healthcare) were used to detect protein signals. Developed membranes were imaged using the ChemiDoc System (Bio-Rad). Selected images were exported and quantified using ImageJ (v.2.0.0).

Cell Culture

$CD8^+$ T cells were isolated from single cell suspensions of spleenocytes and PBMCs from young (3–4 months) or aged (24 months) mice using the $CD8a^+$ T cell Isolation Kit according to manufacturer instructions. Cells were cultured in T cell Media with IL-2 (1:2000, stock 1000 U/μL) at a concentration of 2e6 cells/mL. Three days post culture, media was changed, and cells were incubated with GolgiStop Protein Transport Inhibitor (BD, 554724) at 4 μL/6 mL cell culture for 6 hours to block intracellular protein transport. Cells were then washed and processed for flow cytometry. Endothelial cells were isolated from half brain through liberase (Sigma-Aldrich, 5401119001) digestion at a concentration of 25 μg/mL in digestion buffer (HBSS + HEPES) at 37 degrees C for 45 minutes on a

Please cite this article in press as: Sucharov et al., Aged circulating CD8+ T cells and their secreted factors drive cognitive decline, Immunity (2026), https://doi.org/10.1016/j.immuni.2026.04.014

shaker. The resulting suspension was followed by filtration through a 70 μm. Endothelial cells were then isolated via CD31 antibody and Dynabeads™ Protein G immunoprecipitation Kit (ThermoFisher Scientific, 10007D). The resulting cells were plated on CollagenI coated plates at a concentration of 2E5/mL in Endothelial Cell Media (DMEM + 10% FBS + 1% p/s + 1X ECGS (Cell Applications, 212-GS))

GZMK ELISA

Mouse blood was collected by intracardial bleed at time of euthanasia. Blood was collected with EDTA, followed by centrifugation at 1,000*g* for 10 minutes for plasma separation. For ELISA analysis, plasma was aliquoted and stored at −80 °C until use. GZMK plasma protein concentration was measured by ELISA (MyBioSource, MBS453082) according to the manufacturer's protocol.

HDTVI

GZMK (OriGene, #MR215106), CCL5 (OriGene, #MG227153), and GFP control plasmids were used for HDTVI-mediated systemic overexpression. Hydrodynamic tail vein injections were performed as previously described.[30,61] Endotoxin-free plasmids were prepared using the Qiagen Maxi-Prep Plus Kit (cat# 12963, VWR). GZMK, CCL5, or GFP plasmid DNA (50 ug) was suspended in 3 mL saline and injected in the tail vein in 5–7 seconds in mice. All coding plasmid sequences were verified by Sanger sequencing. To confirm systemic overexpression, mice were injected with HiBiT-tagged GZMK or GFP. The NEBaseChanger tool was used in combination with the Q5 Site-directed Mutagenesis kit (NEB # E0554S) to generate the C-terminally tagged Gzmk construct. The 33 nucleotides coding for the 11 amino acid HiBiT tag were inserted between the last coding and stop codon. Briefly, the HiBiT coding sequence was split between the forward and reverse primers, the plasmid amplified, ligated and transformed according to the manufacturer's instructions. The resulting plasmid was sequence verified using whole plasmid sequencing and amplified using an endotoxin free maxiprep kit. To perform HDTVI of constructs, plasmid DNA (50 μg) was suspended in 3 ml saline and injected in the tail vein in 5–7 seconds in mice. At 24 hours after HDTVI, the mice were euthanized, and plasma was collected by intracardial bleed. A total of 20 μg of protein from each sample was loaded in duplicate in an opaque 96-well plate (Corning, 353296). HiBiT luminescence was measured on the Cytation 5 (BioTek) using the Nano-Glo HiBiT Lytic Detection System (Promega, N3030) according to the manufacturer's instructions.

Retrovirus production

Retroviral GZMK and GFP expression transfer plasmids were generated using the NEBuilder HiFi DNA Assembly Kit (NEB #E5520S), following the manufacturer's recommended design considerations and protocol. Briefly, the MSCV vector backbone (Addgene #127890) was digested with the restriction enzymes EcoRI and BglII and gel purified. eGFP and murine Gzmk coding sequences were PCR amplified with primer sets that included a 20 nucleotide overlap with the backbone and preserved the restriction sites. Additionally, a Kozak sequence was included in the forward primers. All plasmids were sequence verified using whole plasmid sequencing. HEK293T cells were lipotransfected with 40 μL Lipofectamine 3000 in 500 μL OptiMEM, mixed with equal amounts of 7.5 μg pCL-Eco, 7.5 μg retroviral GZMK or GFP, and 36 μL P3000 in 500 μL OptiMEM. 1 mL of transfection mix was added to 7 mL of 293T cells. After 48 and 72 hours, retrovirus-containing media was centrifuged for 5 min at 300 RCF and filtered through 45μm filter to remove cellular debris. Retrovirus was concentrated 100X using lenti-X concentrator (Takara #631232), according to manufacturer instructions. Concentrated retrovirus was used at a dilution of 1:10.

Retroviral overexpression of GZMK and GFP – Isolated CD8+ T cells were cultured in T cell Media + IL-2 (1:2000, stock 1000 U/μL) and activated for 24 hours with Mouse T-Activator CD3/CD28 beads (Gibco, 11452D). 24 hours post activation, cells were resuspended at 2e6 cells/mL in T cell Media + IL-2 (1:1000) + polybrene (10 μg/mL) and seeded on a retronectin coated 12 well plate (15 μg/mL in PBS, Takara, #T100A). Equal volumes of retrovirus or vehicle in T Cell Media (1:10) was added per well. Cells were centrifuged at 2000 RCF for 60 minutes at 30 degrees C and incubated overnight. Media was changed the next day, then subsequent days to allow for proper expansion (reseeding cells at a density of 2e6 cells/mL). Transduction efficiency was analyzed by flow cytometry. 4 days post spinoculation, ½ the aged GFP+ CD8+ T cells were treated with PTx as described above. 24 hours post treatment, cells were washed and resuspended at a density of 3e5 cells/100 μL in saline for adoptive transfer via tail vein injection.

NOR

The NOR task was performed as previously described.[14,30] On day one (the habituation phase), mice performed open field testing by exploring an empty arena for 10 min. Infrared photobeam breaks were recorded and movement metrics were analyzed using the MotorMonitor software (Kinder Scientific). On day two (the training phase), two identical objects were placed into the habituated arena, and the mice were allowed to explore for 5 min. On day three (the testing phase), one object was replaced with a novel object, and the mice were allowed to explore for 5 min. The time spent exploring each object was quantified using the Smart Video Tracking Software (Panlab; Harvard Apparatus). Two different sets of objects were used. To control for any inherent object preference, half of the mice were exposed to object A as their novel object and half to object B. To control for any potential object-independent location preference, the location of the novel object relative to the trained object was also counterbalanced. To determine the percentage of time with the novel object, we calculate (time with novel object)/ (time with trained object + time with novel object) × 100. Mice that did not explore both objects during the training phase were excluded from the analysis.

Please cite this article in press as: Sucharov et al., Aged circulating CD8+ T cells and their secreted factors drive cognitive decline, Immunity (2026), https://doi.org/10.1016/j.immuni.2026.04.014

RAWM

Spatial learning and memory were assessed using the RAWM paradigm, according to an established protocol.[60,62] In this task, the mouse was trained to the location of a constant goal arm throughout the training and testing phase. The start arm changed each trial. Entry into an incorrect arm was scored as an error, and errors were averaged over training blocks (three consecutive trials). During training (day 1), the mice were trained for 12 trials (blocks 1–4), with trials alternating between a visible and hidden platform. After an hour break, learning was tested for 3 trials (block 5) using only a hidden platform. During testing (day 2), the mice were tested for 15 trials (blocks 6–10) with a hidden platform. When scoring, investigators were blinded to treatment. All blocks were analyzed for significance via two-way ANOVA with Šídák's post-hoc, and only significant data points were annotated on figures. Brackets represent significance of area under the curve.

Y maze

The Y Maze task was conducted as previously described.[30] During the training phase, the mice were placed into the start arm facing the wall and were allowed to explore the start and trained arm for 5 min, while the entry to the 3rd arm (novel arm) was blocked. The maze was cleaned between each mouse to remove odor cues, and the trained arm was alternated between mice. After training, the mouse was returned to its home cage. After 45 min, the mouse was returned to the start arm and was allowed to explore all three arms for 5 min. The number of entries in each arm was quantified using the Smart Video Tracking Software (Panlab; Harvard Apparatus). The percentage of entries in each arm was defined as the number of entries in each arm divided by the total number of entries in all arms during the first minute of the task. Mice that did not perform three entries during the first minute of testing were excluded.

Fear conditioning

In this task, mice learned to associate the environmental context (fear conditioning chamber) with an aversive stimulus (mild foot shock; unconditioned stimulus) enabling testing for hippocampal-dependent contextual fear conditioning. To assess amygdala-dependent cued fear conditioning, the mild foot shock was paired with a light and tone cue (conditioned stimulus). Freezing behavior was used as a readout of conditioned fear. Specific training parameters were as follows: tone duration of 30 s; level of 70 dB, 2 kHz; shock duration of 2 s; intensity of 0.6 mA. This intensity is not painful and can easily be tolerated but will generate an unpleasant feeling. On the training day (day 1), each mouse was placed in a fear-conditioning chamber and was allowed to explore for 2 min, during which time freezing was recorded to assess the baseline freezing behavior. Subsequently, a 30 s tone (70 dB) and light, ending with a 2 s foot shock (0.6 mA) were delivered. Then, 2 min later, a second unconditioned-stimulus–conditioned-stimulus pair was delivered. On the testing day (day 2), each mouse was first placed into the fear-conditioning chamber containing the same context, but with no CS or foot shock. Freezing was recorded for 2 min. Freezing was analyzed for 2 min using a FreezeScan video tracking system and software (Cleversys).

QUANTIFICATION AND STATISTICAL ANALYSIS

Data, statistical analyses, and reproducibility

All experiments were randomized and blinded by an independent researcher. Researchers remained blinded throughout histological, biochemical and behavioral assessments. Groups were unblinded at the end of each experiment on statistical analysis. Data are expressed as mean ± S.E.M. The distribution of data in each set of experiments was tested for normality using the D'Agostino–Pearson omnibus test or Shapiro-Wilk test. Statistical analysis was performed using Prism (GraphPad). Means between two groups were compared using two-tailed unpaired Student's *t*-tests. Comparisons of means from multiple groups with each other were analyzed using one-way ANOVA followed by the appropriate post hoc test, as indicated in the figure legends. Additional statistical details are indicated in the respective figure legends. All data generated or analyzed in this study are included in this article. All measurements were taken from distinct samples. Data files for bulk RNA-sequencing (Accession: GSE GSE266454), CITE-sequencing (Accession: GSE GSE266467), and single nucleus RNA-sequencing (Accession: GSE GSE266468) have been uploaded to GEO repository.